STRUCTURAL-ENTROPY-BASED SAMPLE SELECTION FOR EFFICIENT AND EFFECTIVE LEARNING

Anonymous authors
Paper under double-blind review

ABSTRACT

Sample selection improves the efficiency and effectiveness of machine learning models by providing informative and representative samples. Typically, samples can be modeled as a sample graph, where nodes are samples and edges represent their similarities. Most existing methods are based on local information, such as the training difficulty of samples, thereby overlooking global information, such as connectivity patterns. This oversight can result in suboptimal selection because global information is crucial for ensuring that the selected samples well represent the structural properties of the graph. To address this issue, we employ structural entropy to quantify global information and losslessly decompose it from the whole graph to individual nodes using the Shapley value. Based on the decomposition, we present **S**tructural-**E**ntropy-based sample **S**election (**SES**), a method that integrates both global and local information to select informative and representative samples. SES begins by constructing a kNN-graph among samples based on their similarities. It then measures sample importance by combining structural entropy (global metric) with training difficulty (local metric). Finally, SES applies importance-biased blue noise sampling to select a set of diverse and representative samples. Comprehensive experiments in three learning scenarios — supervised learning, active learning, and continual learning — clearly demonstrate the effectiveness of our method.

1 INTRODUCTION

Data budgets that limit sample sizes are pervasive in machine learning applications. For example, researchers and practitioners often face limited annotation and computational resources, necessitating the use of fewer samples to enhance efficiency. Similarly, in continual learning scenarios (Hou et al., 2019), the memory constraint requires fewer samples from previous tasks to effectively retain knowledge. Consequently, effective sample selection becomes crucial to improving efficiency and effectiveness in machine learning. It aims to select informative and representative samples from large datasets to accelerate training and enhance the training performance. Informative samples are those that significantly reduce model uncertainty and are crucial for improving the accuracy and robustness of the training process, while representative samples are those that preserve the diversity and overall distribution of the dataset (Huang et al., 2014). During selection, samples can be modeled as a sample graph, where nodes are samples and edges represent their similarities. Existing sample selection methods primarily focus on local information, such as the training difficulty and the node degree (Maharana et al., 2024). Although these methods demonstrate promising performance on many datasets, they overlook the global information inherent in the graph structure. This global information, such as connectivity patterns, captures the structural properties of the whole graph (Leskovec & Faloutsos, 2006) and has been shown to be effective in improving the representativeness of selected samples (Zhang et al., 2023; Yuan et al., 2021; Zhao et al., 2021). Therefore, we aim to incorporate global information into the sample selection process to improve the quality of the selected samples.

The key to incorporating global information is to identify which specific metric(s) can accurately capture the global structure of the sample graph. Entropy is a class of metrics well-suited for this purpose, as it quantifies both informativeness and representativeness (Pan et al., 2005; Li & Guo, 2013). In particular, Li & Pan (2016) propose structural entropy to evaluate the amount of information required to describe a given graph structure. The main feature of this metric is that it is robust and sensitive. First, it remains stable against minor changes like the addition or removal of a few edges. This ensures that the structural entropy reliably reflects the global structure of the graph despite

potential noise. Second, it is sensitive to topological changes, especially those affecting connectivity patterns. This is essential for capturing the global structure in response to even small topological changes. These two properties make structural entropy an effective metric for quantifying the global structure and therefore valuable in sample selection. However, existing methods only provide a single value for the whole graph. This presents a challenge in decomposing this metric to the level of individual nodes, limiting its utility for fine-grained, node-level selection.

To address this challenge, we use the Shapley value (Shapley, 1951), a method that fairly decomposes a metric among contributors based on their individual contributions. Specifically, it is calculated by evaluating a node's marginal contribution to structural entropy when adding this node to each subgraph of the sample graph. This decomposition process is highly time-consuming as it requires exponential-time computation to enumerate possible subgraphs. To accelerate this, we reformulate the Shapley value for structural entropy, enabling linear-time calculation with respect to the edge number. Based on this reformulation, we propose a node-level structural entropy metric that effectively measures the importance of nodes in preserving the global structure. Building on the decomposition, we present a **S**tructural-**E**ntropy-based sample **S**election (SES) method that integrates both global and local metrics to select informative and representative samples. This method begins by constructing a kNN-graph among samples to describe their similarity relationships. Then, it measures sample importance by combining node-level structural entropy (global metric) with training difficulty (local metric). Finally, the importance-biased blue noise sampling method is employed to iteratively select a set of diverse and representative samples.

We validate the effectiveness of our method through comprehensive experiments on three important learning scenarios: supervised learning, active learning, and continual learning. The evaluation covers many tasks, including image classification, text classification, object detection, and visual question answering. The results clearly show that our method consistently improves state-of-the-art methods across all scenarios and tasks. This indicates that our method of integrating global and local information outperforms existing methods in selecting more informative and representative samples.

The main contributions of this work are threefold:

- We propose a node-level structural entropy metric that quantifies the importance of nodes in preserving the global structure, and it can be calculated in linear time.
- We develop a structural-entropy-based sample selection method that integrates both global and local metrics to select informative and representative samples[1].
- We conduct experiments in supervised learning, active learning, and continual learning that demonstrate the effectiveness of our method.

2 Related work

Existing sample selection methods primarily utilize local information. They can be classified into two categories based on the information utilized: attribute-based methods and connection-based methods.

Attribute-based methods rely on the attributes of individual samples. A commonly used attribute is the training difficulty, which is typically assessed from two perspectives: confidence and error. Metrics that measure model confidence include the entropy of the prediction vector (Coleman et al., 2020) and the variance of the predicted probabilities across training epochs (Swayamdipta et al., 2020). Metrics that measure model error include EL2N (Paul et al., 2021), which calculates the L_2 norm of the error vector, and the Forgetting score (Toneva et al., 2019), which tracks the frequency of misclassifications after initial correct classifications. AUM (Pleiss et al., 2020) combines both perspectives by measuring the confidence for correct classifications and the error for misclassifications. Based on these metrics, several sample selection methods have been developed. One simple yet effective method is selecting the most difficult samples, as they have a larger impact on the model performance (Paul et al., 2021). However, this method overlooks easy samples, which are crucial for model training when data budgets are limited (Sorscher et al., 2022). To address this issue, CCS (Zheng et al., 2022) divides the dataset into strata based on training difficulty and performs random sampling within each stratum. InfoBatch (Qin et al., 2023) retains some easy samples and enhances their influence by upscaling their gradient. Another line of work uses the gradient as the attribute and aims to match the average

[1]The implementation is available at https://anonymous.4open.science/r/SE-based_sample_selection-575B/.

gradient of the selected samples with that of all samples (Mirzasoleiman et al., 2019; Killamsetty et al., 2021). However, these gradients depend on the model's current state during training, limiting the applicability of the selected samples to other models.

Connection-based methods utilize local connections within the sample graph to optimize sample diversity and coverage. GraphCut (Iyer et al., 2021) selects samples with weak connections among them to promote diversity while maintaining strong connections to unselected samples for better coverage. Moderate coreset (Xia et al., 2023) selects samples based on their distances from the class centers. To enhance the generalizability across different scenarios, samples near the median distance are selected. $\mathbb{D}^2$ Pruning (Maharana et al., 2024) aims to select difficult and diverse samples. It employs forward message passing to integrate training difficulty and node degree, followed by backward message passing to ensure diversity.

While these methods demonstrate promising performance on many datasets, they often overlook the global information, which is crucial for increasing the representativeness of selected samples (Yuan et al., 2021). Overlooking this global information can lead to suboptimal learning performance. To address this gap, we propose a structural-entropy-based sample selection method that integrates both global and local metrics to select informative and representative samples. The experimental results presented in Sec. 5 show that our method achieves consistent improvement over existing methods.

3 Background: Structural Entropy of Graph

Structural entropy evaluates how the nodes and edges in a graph are hierarchically organized to form communities at different levels (Li & Pan, 2016). Thus, it is effective in globally quantifying the community structure of the graph regarding its overall connectivity patterns. The calculation of structural entropy is based on an encoding tree that represents the graph's hierarchical community structure. In this tree, each node represents a community, and each leaf node corresponds to a graph node that forms a single-node community. With this encoding tree, the entropy is aggregated across communities of different levels, which provides insights into the hierarchical community structure of the graph. Fig. 1 shows an undirected, weighted graph G and its encoding tree $\mathcal{T}$. The entropy is calculated for each non-root node α, which considers both intra-community and inter-community connections to reflect the connectivity patterns of its community in the graph. Lower entropy indicates denser intra-community connections and sparser inter-community connections. The intra-community connection, $vol(\alpha)$, is quantified by the total weighted degrees of the nodes, while the inter-community connection, $g(\alpha)$, is quantified by the total weight of the edges with exactly one endpoint in the community (outer edges). Given an encoding tree $\mathcal{T}$, the structural entropy of G is the aggregation of the entropy values from all its non-root nodes:

$$\mathcal{H}(G, \mathcal{T}) = -\sum_{\alpha \in \mathcal{T}} \frac{g(\alpha)}{vol(V)} \log \frac{vol(\alpha)}{vol(\alpha^-)}, \tag{1}$$

where α is a non-root node, α^- is its parent node, $g(\alpha)$ is the total weight of its outer edges, and $vol(V)$, $vol(\alpha)$, $vol(\alpha^-)$ represent the total weighted degrees of the nodes in V, α, and α^-.

In real-world applications, the encoding tree $\mathcal{T}$ may be unknown. To best capture the hierarchical community structure in such cases, the encoding tree $\mathcal{T}$ is constructed by minimizing the structural entropy. Obtaining an exact solution for the minimization is challenging, so greedy methods similar to the Huffman tree construction have been developed (Li & Pan, 2016; Zhu et al., 2023). We demonstrate in Appendix A that the choice of the construction method has a negligible effect on the sample selection results. Therefore, we use the most recent method proposed by Zhu et al. (2023).

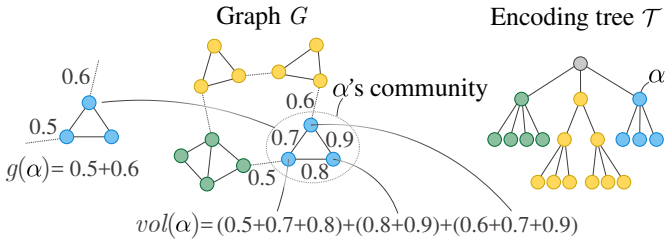

Figure 1: The structural entropy calculation for an undirected, weighted graph.

4 STRUCTURAL-ENTROPY-BASED SAMPLE SELECTION

Our sample selection method integrates global and local metrics to select informative and representative samples. Given a large set of samples, an undirected, weighted sample graph G is initially constructed to model their similarity relationships. Each sample, represented by its embedding extracted by a deep neural network, corresponds uniquely to a node in the graph. To avoid excessive edge connections, each sample is connected to its k nearest neighboring samples. The edge weight between any two samples, u and v, is their cosine similarity normalized to $[0, 1]$. Based on this graph, we first propose a **node-level structural entropy** metric to globally measure the importance of each sample. Then, it is combined with a local metric, training difficulty, to assign an importance score to each sample. Using this score, we develop an **importance-biased blue noise sampling** method to select a set of informative and representative samples.

4.1 NODE-LEVEL STRUCTURAL ENTROPY

The core of our scoring method is to define the metric at the node level. While local metrics are well studied, global metrics have received little attention. An ideal global metric for fine-grained, node-level selection should measure the connectivity patterns of a graph at the individual node level. Previous research shows that the graph-level structural entropy effectively quantifies the global connectivity patterns (Li & Pan, 2016), making it a valuable metric for sample selection. However, it only provides a single value for the whole graph, thus failing to offer detailed insights at the node level. Consequently, the key is to decompose the graph-level structural entropy to the node level.

Chen & Teng (2017) have shown that the Shapley value (Shapley, 1951) is an effective method to decompose a value from the graph level to the node level. The key feature of this method is its lossless and fair decomposition of the value, ensuring that the aggregate node-level value equals the graph-level value. Inspired by this, we employ the Shapley value to derive the node-level structural entropy. Specifically, the Shapley value of a node u reflects the average increase in structural entropy when it is added to all possible subgraphs of G. As a result, this value captures the node's contribution to the global connectivity patterns.

To derive the Shapley value for each node, we first calculate the structural entropy for each possible subgraph of G. Then, we calculate the node's contribution to these subgraphs. Formally, let V_S denote a subset of the node set V, the Shapley value of node u is:

$$\phi(u) = \frac{1}{|V|} \sum_{V_s \subseteq V \setminus \{u\}} \binom{|V|-1}{|V_S|}^{-1} \Big(\mathcal{H}(G[V_S \cup \{u\}], \mathcal{T}) - \mathcal{H}(G[V_S], \mathcal{T}) \Big), \tag{2}$$

where $G[V_S]$ is the subgraph of G that consists of nodes in V_S and the edges between them, and $\binom{|V|-1}{|V_S|}$ is the binomial coefficient.

Directly calculating Eq. (2) requires an enumeration of all possible subgraphs of G, which becomes intractable for a graph with a large number of nodes. To address this, we reformulate the Shapley value by considering the contribution of edges.

Proposition 1. *Let $G = (V, E, W)$ be an undirected, weighted graph. The Shapley value of node u is*

$$\phi(u) = \frac{1}{vol(V)} \left(\sum_{\langle u,v \rangle \in E} w_{u,v} \log vol(\alpha_{u \vee v}) - d(u) \log d(u) \right), \tag{3}$$

where $w_{u,v}$ is the weight of edge $\langle u, v \rangle$, $\alpha_{u \vee v}$ is the least common ancestor of node u and v in the encoding tree $\mathcal{T}$, and $d(u)$ is the weighted degree of node u.

The proof of Proposition 1 is provided in Appendix B. It indicates that the Shapley value can be calculated in linear time with respect to the edge number. Thus, this reformulation enables an efficient and exact calculation. Eq. (3) consists of two terms. The first decomposes the structural entropy from the encoding tree to the node, and the second reflects local connectivity through node degree. Due to the below theoretical and empirical advantages, we only use the first term to define the node-level structural entropy (S_e):

$$S_e(u) = \frac{1}{vol(V)} \sum_{\langle u,v \rangle \in E} w_{u,v} \log vol(\alpha_{u \vee v}). \tag{4}$$

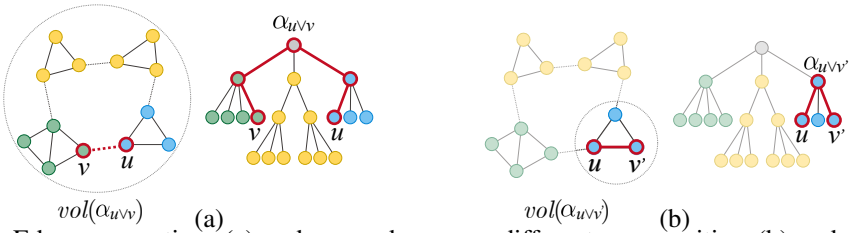

Figure 2: Edges connecting: (a) nodes u and v across different communities; (b) nodes u and v' within the same community.

As this definition is related to sample coverage, the first theoretical advantage lies in its ability to enhance model performance. Following previous work (Zheng et al., 2022), we assume that samples are drawn from a distribution P_μ with probability measure μ, and quantify the sample coverage as $P(u,r) = \int_{B(u,r)} d\mu(x)$, where $B(u,r)$ is a r-radius ball centered at u. We prove that $S_e(u)$ provides a lower bound for sample coverage:

$$\frac{1}{nk^2R}\exp\left(\frac{1}{kR}\mathbb{E}[S_e(u)]\right) \leq \mathbb{E}[P(u,r)], \tag{5}$$

where n is the number of samples, k is the parameter in kNN-graph construction, and R is the upper bound of edge weights. This result indicates that maximizing $S_e(u)$ during selection inherently improves sample coverage. Given the strong correlation between coverage ability and the empirical loss of a learning algorithm (Zheng et al., 2022), selecting samples with high node-level structural entropy effectively enhances model performance. The detailed proof is provided in Appendix C.

The second theoretical advantage is its ability in maintaining the overall graph structure. A higher $vol(\alpha_{u\vee v})$ indicates that the edge $\langle u, v\rangle$ connects nodes that are more distantly located in $\mathcal{T}$. For example, in Fig. 2, the edge $\langle u, v'\rangle$ stays within the same community while the edge $\langle u, v\rangle$ spans different communities, resulting in a higher $vol(\alpha_{u\vee v})$. Thus, $vol(\alpha_{u\vee v})$ effectively quantifies the extent to which an edge bridges different communities. Since $S_e(u)$ is the weighted sum of $vol(\alpha_{u\vee v})$, nodes with high structural entropy serve as boundaries between communities. Selecting these nodes is crucial for maintaining the overall structure of the graph.

The empirical advantage of this definition is demonstrated through an ablation study, as detailed in Appendix G. The results show that only using the first term slightly improves performance.

4.2 Importance-Biased Blue Noise Sampling

To select a set of high-quality samples, the developed global metric, node-level structural entropy, needs to be combined with an appropriate local metric. Previous research has shown that training difficulty (S_t) is an effective local metric in quantifying the sample's impact on model performance, as difficult samples are typically more informative for improving the decision boundary (Paul et al., 2021; Sorscher et al., 2022). Therefore, we employ it as the local metric. Accordingly, the overall importance score (S) is a combination of node-level structural entropy and training difficulty:

$$S(u) = S_e(u) \cdot S_t(u). \tag{6}$$

Given the importance scores, a straightforward solution is to select the samples with the highest scores. However, this significantly reduces the diversity of the selected samples, as the important samples tend to cluster in several narrow regions (Zheng et al., 2022). An alternative is the message passing mechanism employed by $\mathbb{D}^2$ Pruning: once a sample is selected, this method sends weighted messages to decrease the importance scores of its neighbors in the graph. However, the message weights are sensitive to a hyperparameter and can lead to suboptimal results if not carefully tuned. Previous research has shown that blue noise sampling achieves a good balance between randomness and uniformity by excluding overly similar samples (Xiang et al., 2019; Liu et al., 2018). This method increases sampling in low-density regions, which enhances the diversity of the selected samples. Consequently, we develop an importance-biased blue noise sampling method to select a set of informative and representative samples.

Our sampling process contains two steps: 1) identifying the candidate sample with the highest importance score, 2) rejecting the sample if its similarity with any selected neighboring samples exceeds a threshold θ; otherwise, accepting it as a selected sample. These two steps are performed iteratively until no more samples can be selected. To determine the threshold θ for a given sampling rate, we perform a binary search on θ.

5 EXPERIMENTS

In this section, we first demonstrate the effectiveness of our method in three learning scenarios: supervised learning, active learning, and continual learning. We then conduct ablation studies to provide insights into our method. Finally, we conduct a qualitative analysis of the selection results.

5.1 SUPERVISED LEARNING

In supervised learning tasks, including image classification, text classification, object detection, and visual question answering, we aim to reduce computational costs by selecting a subset of informative and representative samples for training.

5.1.1 EXPERIMENTAL SETUP

Datasets and models. For image classification, we use the widely used datasets, CIFAR10, CIFAR100 (Krizhevsky, 2009), and ImageNet-1K (Deng et al., 2009). Following Maharana et al. (2024), ResNet-18 (He et al., 2015) is used for CIFAR10 and CIFAR100, while ResNet-34 (He et al., 2015) is used for ImageNet-1K. The models are trained from scratch on the selected subsets of the training set, and we report the model accuracy.

For text classification, we use the ANLI dataset (Nie et al., 2020), which focuses on natural language inference, and the IMDB Review dataset (Maas et al., 2011), which focuses on sentiment analysis. Following Maharana et al. (2024), we fine-tune the RoBERTa model (Liu et al., 2019) and report the accuracy on the test set for both datasets.

For object detection, we use the PASCAL VOC dataset (Everingham et al., 2010), which contains bounding box annotations of objects and animals. Following Choi et al. (2021), we train SSD (Liu et al., 2016) with VGG-16 (Simonyan & Zisserman, 2015) backbone from scratch and report the mAP on the test set.

For visual question answering, we use the CC SBU Align dataset (Zhu et al., 2024), which contains high-quality, aligned image-text pairs. Following Wei et al. (2023), we fine-tune MiniGPT-4 (Zhu et al., 2024) on this dataset, and report the average accuracy of the model on five datasets: OKVQA (Schwenk et al., 2022), IconVQA (Lu et al., 2021), DocVQA (Mathew et al., 2021), GQA (Hudson & Manning, 2019), and ScienceQA (Saikh et al., 2022).

Please refer to Appendix D for more details on the dataset statistics and training hyperparameters.

Baselines. We compare our method with the state-of-the-art sample selection methods, which are either applicable to all tasks or designed for a specific task. Baselines that are applicable to all tasks include: 1) **Random** selection of samples, 2) **Moderate** coreset (Xia et al., 2023), 3) **CCS** (Zheng et al., 2022), 4) $\mathbb{D}^2$ **Pruning** (Maharana et al., 2024), and 5) **GraphCut** (Iyer et al., 2021). For image classification and text classification, the task-specific baselines include selecting the most difficult samples based on: 1) **Entropy** (Coleman et al., 2020), 2) **Forgetting** score (Toneva et al., 2019), 3) **EL2N** (Paul et al., 2021), 4) **AUM** (Pleiss et al., 2020), and 5) **Variance** (Swayamdipta et al., 2020). We also include two widely used baselines that prioritize diversity in sample selection, including ***k*-means** (Xu et al., 2003), which selects the samples closest to k-means clustering centers, and ***k*-DPP** (Kulesza & Taskar, 2011), which employs a determinantal point process to encourage diversity. For object detection, we include selection based on the **AL-MDN** uncertainty (Choi et al., 2021), which captures the detector's overall uncertainty for an image. For visual question answering, we include selection based on the **Instruction** score (Wei et al., 2023), which evaluates an image-text pair based on image-text matching degree and text length.

Implementation. For all tasks, we extract image embeddings using CLIP (Radford et al., 2021) and text embeddings using Sentence-BERT (Reimers & Gurevych, 2019) due to their demonstrated performance in capturing the semantic similarities across various domains. For visual question answering, we concatenate the image and text embeddings for each sample. To measure training difficulty, we use AUM for image classification, Variance for text classification, AL-MDN uncertainty for object detection, and Instruction score for visual question answering. We ablate the different training difficulty metrics in Sec. 5.4 and observe that there is no significant performance difference among them. We also perform a grid search on the hyperparameters, such as k in the kNN-graph construction (see Appendix E for details).

Table 1: Results for supervised learning on: (a) ImageNet-1K; (b) ANLI; (c) PASCAL VOC; (d) CC SBU Align. The best one is **bold**, and the runner-up is underlined.

(a) ImageNet-1K

Dataset	ImageNet-1K (100%:73.63)						
Sampling rate	70%	50%	20%	10%	5%	2%	1%
Random	71.63	69.26	58.90	47.10	34.04	16.56	5.50
Moderate	71.33	68.72	55.23	40.97	25.75	11.33	4.52
CCS	70.74	69.23	60.04	50.41	36.92	19.92	9.43
$\mathbb{D}^2$ Pruning	71.29	70.32	58.91	50.81	37.12	18.97	11.23
GraphCut	68.91	68.72	55.28	44.79	33.54	20.07	11.49
Entropy	70.93	69.21	54.76	38.46	22.78	7.01	1.95
Forgetting	70.57	70.46	60.77	48.73	33.86	15.13	5.66
EL2N	71.68	65.98	31.90	12.57	6.50	3.25	1.90
AUM	69.94	65.36	21.91	10.50	6.42	3.58	2.24
Variance	70.12	66.09	35.15	13.85	7.13	4.72	1.81
***k*-means**	70.33	69.47	59.23	48.12	35.51	18.67	9.65
***k*-DPP**	70.84	69.85	59.92	46.10	34.41	16.33	7.49
SES (Ours)	**72.80**	**71.05**	**63.24**	**53.59**	**41.88**	**25.59**	**13.43**

(b) ANLI

Dataset	ANLI (100%:49.25)						
Sampling rate	70%	50%	20%	10%	5%	2%	1%
Random	47.08	45.20	42.13	39.52	38.82	37.50	35.96
Moderate	46.84	45.11	41.95	40.16	38.99	35.83	33.91
CCS	46.56	45.92	41.67	41.63	40.33	37.41	36.82
$\mathbb{D}^2$ Pruning	48.56	47.49	42.77	41.43	40.34	37.92	36.29
GraphCut	46.14	44.53	42.12	39.86	38.15	35.44	34.02
Entropy	46.32	45.53	41.45	39.67	38.54	36.69	36.40
Forgetting	48.73	42.29	39.82	38.37	35.95	35.78	35.03
EL2N	48.70	47.85	43.14	39.63	37.52	34.33	34.27
AUM	47.86	47.58	43.57	40.02	34.66	34.16	33.62
Variance	47.97	47.87	40.70	38.75	33.52	33.50	33.17
***k*-means**	46.48	46.52	42.42	40.57	39.89	36.74	36.11
***k*-DPP**	47.74	47.02	43.44	40.98	40.12	37.44	36.66
SES (Ours)	**49.00**	**48.22**	**45.94**	**43.63**	**41.82**	**39.88**	**38.16**

(c) PASCAL VOC

Dataset	PASCAL VOC (100%:76.29)						
Sampling rate	70%	50%	20%	10%	5%	2%	1%
Random	74.02	72.10	65.45	57.56	43.47	18.78	9.24
Moderate	73.42	72.03	65.12	54.71	40.20	15.97	5.13
CCS	74.64	72.27	65.72	57.35	39.01	17.26	8.49
$\mathbb{D}^2$ Pruning	74.46	72.55	65.59	55.73	44.04	19.16	10.75
GraphCut	67.45	64.15	53.12	38.29	26.81	8.56	8.16
AL-MDN	74.51	70.36	65.26	54.51	30.85	12.33	8.97
***k*-means**	74.22	72.35	65.52	57.01	43.35	16.96	5.16
***k*-DPP**	74.19	71.99	65.39	56.80	43.92	18.20	10.50
SES (Ours)	**75.20**	**73.33**	**66.52**	**59.52**	**45.92**	**23.39**	**16.15**

(d) CC SBU Align

Dataset	CC SBU Align (100%:30.40)						
Sampling rate	70%	50%	20%	10%	5%	2%	1%
Random	29.66	29.62	29.21	29.01	28.20	25.51	25.11
Moderate	29.96	29.67	29.53	29.11	27.30	24.85	26.54
CCS	29.93	29.90	29.94	29.91	27.71	25.31	25.59
$\mathbb{D}^2$ Pruning	30.09	29.97	29.44	29.30	26.44	25.03	26.29
GraphCut	29.86	29.73	29.53	29.11	27.30	24.85	26.54
Instruction	30.12	29.93	29.82	29.01	26.76	23.72	24.60
***k*-means**	29.78	29.61	29.54	29.20	27.72	25.47	25.60
***k*-DPP**	29.33	29.55	29.48	29.27	28.16	25.93	26.13
SES (Ours)	**30.25**	**30.20**	**30.21**	**30.10**	**28.23**	**27.19**	**27.61**

5.1.2 RESULTS

To cover a wide range of sampling rates, we select subsets that contain 1%, 2%, 5%, 10%, 20%, 50%, and 70% of the entire training set. All the results are averaged over 5 random seeds. Table 1 shows the results on four datasets that cover all the four tasks. The full results are provided in Appendix F.

Baselines that select the most difficult samples, such as AUM and Forgetting, perform well in high-sampling-rate settings. However, these methods fall behind in low-sampling-rate settings. This is due to their limited coverage of easy samples, which are crucial for model training when fewer samples are selected (Sorscher et al., 2022). Methods that prioritize sample coverage, such as CCS and $\mathbb{D}^2$ Pruning, address this issue and perform well in low-sampling-rate settings. However, in high-sampling-rate settings, they cannot accurately determine the most important samples that preserve global structure. This results in a lack of representativeness in the selected samples and suboptimal performance. Methods that prioritize diversity are competitive in low-sampling-rate settings because they ensure the coverage of the dataset. However, in high-sampling-rate settings, they face challenges in balancing diversity with sample importance, leading to suboptimal performance. In contrast, our method integrates both global and local metrics to better identify important samples and employs importance-biased blue noise sampling to ensure representativeness. Therefore, our method consistently performs better than baselines across all sampling rates and datasets.

In text classification and visual question answering, we observe that decreasing the sampling rate does not significantly affect performance. This is because we are fine-tuning pretrained models, which provide sufficient knowledge for these tasks. By providing high-quality samples, our method significantly accelerates fine-tuning with negligible performance loss. For example, as shown in Table 1(d), we achieve a 10x speedup by using only 10% of the dataset to fine-tune MiniGPT-4, with only a 0.3% drop in accuracy compared to using the entire dataset. Specifically, our method reduces the fine-tuning time on a single Nvidia Tesla V100 GPU from approximately 30 minutes to 3 minutes, adding only a negligible selection overhead of 2 seconds.

5.2 ACTIVE LEARNING

Active learning (Settles, 2009) aims to reduce annotation effort by selecting a set of informative and representative samples from an unlabeled pool. These samples are then labeled to train models. The key difference between active learning and supervised learning lies in the absence of labels during sample selection, which makes the selection process more challenging.

Table 2: Results for active learning. The best one is **bold**, and the runner-up is underlined.

Dataset	ImageNet-1K (100%:73.63)						
Sampling rate	70%	50%	20%	10%	5%	2%	1%
Random	71.12	69.43	58.77	47.36	33.41	16.41	5.41
Moderate	71.48	68.68	56.35	42.29	26.77	11.37	4.22
CCS	71.46	69.50	58.85	45.06	28.02	9.03	2.33
GraphCut	71.50	69.16	56.08	40.99	24.30	7.90	2.46
$\mathbb{D}^2$ **Pruning**	71.62	69.02	59.65	45.97	28.08	14.24	4.79
Prototypicality	70.12	66.00	49.20	35.27	24.14	13.88	4.95
SES (Ours)	**72.11**	**70.15**	**60.22**	**48.10**	**34.82**	**17.97**	**6.69**

5.2.1 Experimental Setup

Datasets and models. To evaluate the effectiveness of the selection methods in an active learning task, we perform image classification on ImageNet-1K. To simulate an unlabeled pool, we remove the labels from all samples during selection. After selection, we use the ground-truth labels to simulate human annotations. We train ResNet-34 from scratch on these labeled images and report the accuracy on the ImageNet-1K validation set.

Baselines. We include the baselines from Sec. 5.1 that are applicable to unlabeled datasets: 1) **Random**, 2) **CCS**, 3) $\mathbb{D}^2$ **Pruning**, and 4) **GraphCut**. Additionally, we include **Prototypicality** (Sorscher et al., 2022) designed for unlabeled datasets. This method selects the most difficult samples based on the prototypicality score, which is defined as the distance between samples and their corresponding k-means cluster center. Difficult samples are those far from the center, as they tend to be more ambiguous than the samples closer to the center.

Implementation. In the active learning scenario, using a pretrained supervised model like CLIP for feature extraction is not suitable, because the domain of the unlabeled data may not be covered by its pretraining data. Therefore, we extract the image embeddings with a self-supervised model, SwAV (Caron et al., 2020). In the baselines and our method, the prototypicality score is utilized to measure training difficulty.

5.2.2 Results

We select unlabeled samples with rates of 1%, 2%, 5%, 10%, 20%, 50%, and 70% and report the results averaged over 5 random seeds in Table 2. In low-sampling-rate settings, other baselines perform worse than random selection due to the absence of labels, indicating their reliance on labeled data to achieve optimal performance. In contrast, our method consistently performs better than random selection and other baseline methods. This is because structural entropy compensates for missing labels by capturing the community structure in the datasets.

5.3 Continual Learning

Continual learning (Kirkpatrick et al., 2017) aims to alleviate the catastrophic forgetting of previously learned tasks when learning new tasks over time. We focus on the replay-based method (Hou et al., 2019), which selects a small set of informative and representative samples from previous tasks and replays them during the training of new tasks.

5.3.1 Experimental Setup

Datasets and models. We use the datasets commonly used in continual learning, including Permuted MNIST, Split MNIST, Split CIFAR10, Split CIFAR100, and Split Tiny-ImageNet. Permuted MNIST splits MNIST (LeCun et al., 1998) into 10 segments, where a fixed permutation of the pixel order is applied to all images in each segment to simulate different distributions. Thus, it contains 10 classification tasks with samples from different distributions. The other four datasets split the image classes in MNIST, CIFAR10, CIFAR100, and Tiny-ImageNet (Le & Yang, 2015) into 5, 5, 20, and 20 segments, respectively, and each segment corresponds to a different classification task. In alignment with prior studies (Borsos et al., 2020; Hao et al., 2024), we use increasingly complex models as dataset complexity grows: a two-layer MLP for Permuted MNIST, a four-layer CNN for Split MNIST, ResNet-18 for Split CIFAR10, and ResNet-18 with multi-head output (Zenke et al., 2017) for Split CIFAR100 and Split Tiny-ImageNet. Following the class-incremental setting (Wang et al., 2024),

Table 3: Results for continual learning. The best one is **bold**, and the runner-up is underlined.

Dataset	Permuted MNIST		Split MNIST		Split CIFAR10		Split CIFAR100		Split Tiny-ImageNet	
Memory size	100	200	100	200	100	200	100	200	100	200
$\mathbb{D}^2$ **Pruning**	78.25	79.94	96.79	97.69	64.54	66.08	51.86	54.50	19.08	19.50
GraphCut	76.98	78.61	91.34	94.25	61.02	61.66	53.35	54.66	19.76	20.53
***k*-center**	78.17	79.75	94.39	96.61	61.47	62.74	51.16	53.10	18.87	18.90
Gradient Matching	77.30	79.27	95.39	97.54	61.65	62.65	54.13	56.29	19.19	19.00
FRCL	77.33	79.21	94.48	97.10	61.67	62.93	51.40	54.28	18.86	19.01
iCaRL	78.94	80.65	89.50	97.59	62.33	64.08	54.62	56.11	19.58	19.85
Greedy Coreset	78.71	80.13	96.07	97.76	63.18	62.98	56.17	57.72	19.24	19.98
BCSR	77.74	79.51	94.77	96.98	63.23	64.59	50.21	51.49	18.75	18.74
SES (Ours)	**79.92**	**81.18**	**96.94**	**98.28**	**68.26**	**69.32**	**57.60**	**59.69**	**20.80**	**21.20**

the models are trained sequentially for each task while maintaining a fixed-size replay memory that contains an equal number of samples for each previous task. During training, samples from both the replay memory and the current task are used, with the replay samples weighted by a hyperparameter that controls their influence on the current task. After completing each task, a subset of samples is selected from the current task to replace a portion of the replay memory. We report the average accuracy on all tasks, with the model unaware of a sample's task during testing.

Baselines. We include baselines from Sec. 5.1 to select samples that update the replay memory. Additionally, we include six widely used selection methods for continual learning: 1) ***k*-center** (Sener & Savarese, 2018), 2) **Gradient Matching** (Campbell & Broderick, 2019), 3) **FRCL** (Titsias et al., 2020), 4) **iCaRL** (Rebuffi et al., 2017), 5) **Greedy Coreset** (Borsos et al., 2020), and 6) **BCSR** (Hao et al., 2024). Detailed introduction of these methods is provided in Appendix F.

Implementation. Consistent with the implementation in Sec. 5.1, we extract the image embeddings with CLIP and measure training difficulty with AUM. For all baselines and our method, we perform a grid search on the weight of replay samples during training to determine its optimal value (see Appendix D for details).

5.3.2 Results

We test replay memory sizes of 50, 100, 200, and 400 and report the results averaged over 5 random seeds. Due to space limitations, Table 3 shows the results for replay memory sizes of 100 and 200, excluding baselines from Sec. 5.1 that are neither the best nor the runner-up in any dataset or memory size. The full results are provided in Appendix F. Our method consistently achieves better performance than baselines across all memory sizes and datasets. This is because the combination of node-level structural entropy and training difficulty captures both the global structure of samples and the model training dynamics in retaining knowledge.

5.4 Ablation Study

We conduct ablation studies on supervised learning using CIFAR10 to evaluate the impact and behavior of each module in our method. This section presents results on the effect of modules and k in the kNN-graph construction. Additional ablation studies are provided in Appendix G.

Effect of modules. We ablate the two key modules in our method, node-level structural entropy (SE) and importance-biased blue noise sampling (BNS), by replacing them with alternatives. Without SE, we score samples based solely on training difficulty (TD). Without BNS, we either select samples with the highest scores (HS) or use the message passing (MP) method from $\mathbb{D}^2$ pruning. The

Table 4: Ablation of modules. The best one is **bold**, and the runner-up is underlined.

Module		Sampling rate							Avg.
Scoring	Sampling	70%	50%	20%	10%	5%	2%	1%	
TD	HS	94.85	93.90	70.88	60.68	47.36	38.30	32.41	62.63
TD	MP	94.86	94.28	87.88	77.68	65.30	49.69	41.41	73.01
TD	BNS	94.88	94.05	88.06	79.55	68.05	53.37	43.07	74.43
SE+TD	HS	94.92	94.39	82.03	70.42	57.63	40.64	33.68	67.67
SE+TD	MP	**95.08**	**94.67**	**88.54**	80.14	69.34	54.26	44.51	75.22
SE+TD	BNS	95.01	94.50	88.31	**80.24**	**69.82**	**54.78**	**45.25**	**75.42**

hyperparameter controlling message weights in MP is determined through grid search as in the original paper (Maharana et al., 2024). Table 4 shows the results. Using TD and HS yields the lowest performance. Incorporating either SE, BNS, or MP largely improves performance, demonstrating their individual effectiveness. Combining SE with either BNS or MP further improves the performance, indicating that SE complements both methods in selecting informative and representative samples. Notably, BNS achieves comparable performance to MP without the need for the time-consuming grid search on the additional hyperparameter, demonstrating its effectiveness.

Effect of k in the kNN-graph construction. We test the effect of k in the kNN-graph construction. Fig. 3 shows the results when selecting 10% of the samples from CIFAR10. As k increases, the performance first increases and then remains relatively stable within a narrow range. This indicates that the first few nearest neighbors effectively capture the global structure of the samples, which aligns with prior research (Jaffe et al., 2020). Based on the grid search results across datasets, we empirically determine $\log_2 n$ to be an appropriate value for k, where n is the number of samples.

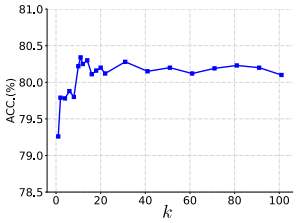

Figure 3: Ablation of k in the kNN-graph construction.

5.5 Qualitative Analysis

We visualize the selection results of different methods when selecting 2% of the samples from CIFAR10 by projecting them onto a two-dimensional plane using t-SNE (van der Maaten & Hinton, 2008). Fig. 4 shows the results of AUM, $\mathbb{D}^2$ Pruning, and our method. Each point is a selected sample, and the colored contours indicate the high-density regions for each class. The full results are provided in Appendix H. Methods that select the most difficult samples, such as AUM, oversample near several class boundaries and undersample in several classes that are easier to classify (Fig. 4(a)). Methods that prioritize sample coverage, such as $\mathbb{D}^2$ Pruning, achieve a better sample coverage but still miss critical samples near class boundaries (Fig. 4(b)). This gap indicates that these methods may not effectively preserve the global structure of the samples. Our method well covers the data distribution, providing a set of informative and representative samples for model training (Fig. 4(c)).

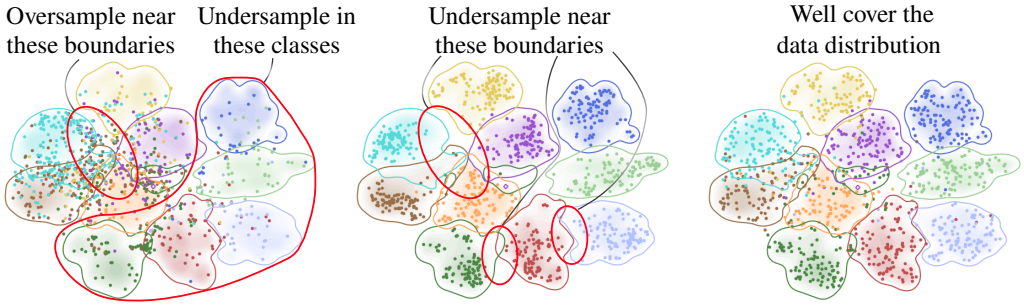

Figure 4: Visualizations of results when selecting 2% of the samples from CIFAR10 using: (a) AUM; (b) $\mathbb{D}^2$ Pruning; (c) our structural-entropy-based sample selection method.

6 Conclusion

In this paper, we present a structural-entropy-based sample selection method for efficient and effective learning. The key idea behind our method is to decompose graph-level structural entropy to a node-level global metric using the Shapley value. This global metric is combined with a local metric, training difficulty, for selecting informative and representative samples. The effectiveness of our method is validated by comprehensive experiments in three learning scenarios. Although our method has proven effective, future work on the following aspects is still promising. First, automating the hyperparameter selection based on data characteristics can reduce the computational costs of the grid search. Second, improving the support for multimodal data could strengthen its performance across a wider range of tasks, such as infographics VQA (Mathew et al., 2022) and building foundation models (Yang et al., 2024). Third, applying techniques such as hyper-class representation (Zhang et al., 2022) to enhance the image and text embeddings can improve the quality of selected samples.

REFERENCES

Sameer Agarwal, Kristin Branson, and Serge Belongie. Higher order learning with graphs. In *Proceedings of the International Conference on Machine Learning*, pp. 17–24, 2006.

Zalán Borsos, Mojmir Mutny, and Andreas Krause. Coresets via bilevel optimization for continual learning and streaming. In *Proceedings of Advances in Neural Information Processing Systems*, pp. 14879–14890, 2020.

Trevor Campbell and Tamara Broderick. Automated scalable bayesian inference via hilbert coresets. *Journal of Machine Learning Research*, 20(15):1–38, 2019.

Mathilde Caron, Ishan Misra, Julien Mairal, Priya Goyal, Piotr Bojanowski, and Armand Joulin. Unsupervised learning of visual features by contrasting cluster assignments. In *Proceedings of Advances in Neural Information Processing Systems*, pp. 9912–9924, 2020.

Wei Chen and Shang-Hua Teng. Interplay between social influence and network centrality: A comparative study on shapley centrality and single-node-influence centrality. In *Proceedings of the international conference on world wide web*, pp. 967–976, 2017.

Jiwoong Choi, Ismail Elezi, Hyuk-Jae Lee, Clement Farabet, and Jose M. Alvarez. Active learning for deep object detection via probabilistic modeling. In *Proceedings of the IEEE/CVF International Conference on Computer Vision*, pp. 10264–10273, 2021.

Cody A. Coleman, Christopher Yeh, Stephen Mussmann, Baharan Mirzasoleiman, Peter D. Bailis, Percy Liang, Jure Leskovec, and Matei A. Zaharia. Selection via proxy: Efficient data selection for deep learning. In *Proceedings of the International Conference on Learning Representations*, 2020.

Jia Deng, Wei Dong, Richard Socher, Li-Jia Li, Kai Li, and Li Fei-Fei. Imagenet: A large-scale hierarchical image database. In *Proceedings of the IEEE/CVF Conference on Computer Vision and Pattern Recognition*, pp. 248–255, 2009.

Mark Everingham, Luc Van Gool, Christopher K. I. Williams, John M. Winn, and Andrew Zisserman. The pascal visual object classes (voc) challenge. *International Journal of Computer Vision*, 88(2): 303–338, 2010.

Yifan Feng, Haoxuan You, Zizhao Zhang, Rongrong Ji, and Yue Gao. Hypergraph neural networks. In *Proceedings of the AAAI conference on artificial intelligence*, pp. 3558–3565, 2019.

Bernd Fritzke. A growing neural gas network learns topologies. In *Proceedings of Advances in Neural Information Processing Systems*, pp. 625–632, 1995.

Samir Yitzhak Gadre, Gabriel Ilharco, Alex Fang, Jonathan Hayase, Georgios Smyrnis, Thao Nguyen, Ryan Marten, Mitchell Wortsman, Dhruba Ghosh, Jieyu Zhang, et al. Datacomp: In search of the next generation of multimodal datasets. *Proceedings of Advances in Neural Information Processing Systems*, 36, 2024.

Chengcheng Guo, Bo Zhao, and Yanbing Bai. Deepcore: A comprehensive library for coreset selection in deep learning. In *Proceedings of International Conference on Database and Expert Systems Applications*, pp. 181–195, 2022.

Jie Hao, Kaiyi Ji, and Mingrui Liu. Bilevel coreset selection in continual learning: A new formulation and algorithm. In *Proceedings of Advances in Neural Information Processing Systems*, pp. 51026–51049, 2024.

Kaiming He, X. Zhang, Shaoqing Ren, and Jian Sun. Deep residual learning for image recognition. In *Proceedings of the IEEE/CVF Conference on Computer Vision and Pattern Recognition*, pp. 770–778, 2015.

Saihui Hou, Xinyu Pan, Chen Change Loy, Zilei Wang, and Dahua Lin. Learning a unified classifier incrementally via rebalancing. In *Proceedings of the IEEE/CVF Conference on Computer Vision and Pattern Recognition*, pp. 831–839, 2019.

Sheng-Jun Huang, Rong Jin, and Zhi-Hua Zhou. Active learning by querying informative and representative examples. *IEEE Transactions on Pattern Analysis and Machine Intelligence*, 36(10): 1936–1949, 2014.

Drew A. Hudson and Christopher D. Manning. GQA: A new dataset for real-world visual reasoning and compositional question answering. In *Proceedings of the IEEE/CVF Conference on Computer Vision and Pattern Recognition*, pp. 6693–6702, 2019.

Rishabh Iyer, Ninad Khargoankar, Jeff Bilmes, and Himanshu Asanani. Submodular combinatorial information measures with applications in machine learning. In *Proceedings of the International Conference on Algorithmic Learning Theory*, pp. 722–754, 2021.

Ariel Jaffe, Yuval Kluger, George C. Linderman, Gal Mishne, and Stefan Steinerberger. Randomized near-neighbor graphs, giant components and applications in data science. *Journal of applied probability*, 57 2:458–476, 2020.

Krishnateja Killamsetty, Durga Sivasubramanian, Ganesh Ramakrishnan, Abir De, and Rishabh K. Iyer. Grad-match: Gradient matching based data subset selection for efficient deep model training. In *Proceedings of the International Conference on Machine Learning*, 2021.

James Kirkpatrick, Razvan Pascanu, Neil Rabinowitz, Joel Veness, Guillaume Desjardins, Andrei A Rusu, Kieran Milan, John Quan, Tiago Ramalho, Agnieszka Grabska-Barwinska, et al. Overcoming catastrophic forgetting in neural networks. *Proceedings of the national academy of sciences*, 114 (13):3521–3526, 2017.

Alex Krizhevsky. Learning multiple layers of features from tiny images. Technical Report TR-2009, University of Toronto, 2009.

Alex Kulesza and Ben Taskar. k-dpps: Fixed-size determinantal point processes. In *Proceedings of the International Conference on Machine Learning*, pp. 1193–1200, 2011.

Ya Le and Xuan Yang. Tiny imagenet visual recognition challenge. *CS 231N*, 7(7):3, 2015.

Yann LeCun, Léon Bottou, Yoshua Bengio, and Patrick Haffner. Gradient-based learning applied to document recognition. *Proceedings of the IEEE*, 86(11):2278–2324, 1998.

Jure Leskovec and Christos Faloutsos. Sampling from large graphs. In *Proceedings of the ACM SIGKDD international conference on Knowledge discovery and data mining*, pp. 631–636, 2006.

Angsheng Li and Yicheng Pan. Structural information and dynamical complexity of networks. *IEEE Transactions on Information Theory*, 62(6):3290–3339, 2016.

Xin Li and Yuhong Guo. Adaptive active learning for image classification. In *Proceedings of the IEEE conference on computer vision and pattern recognition*, pp. 859–866, 2013.

Mengchen Liu, Jiaxin Shi, Kelei Cao, Jun Zhu, and Shixia Liu. Analyzing the training processes of deep generative models. *IEEE transactions on visualization and computer graphics*, 24(1):77–87, 2018.

Wei Liu, Dragomir Anguelov, Dumitru Erhan, Christian Szegedy, Scott Reed, Cheng-Yang Fu, and Alexander C Berg. Ssd: Single shot multibox detector. In *Proceedings of European Conference on Computer Vision*, pp. 21–37, 2016.

Yinhan Liu, Myle Ott, Naman Goyal, Jingfei Du, Mandar Joshi, Danqi Chen, Omer Levy, Mike Lewis, Luke Zettlemoyer, and Veselin Stoyanov. Roberta: A robustly optimized bert pretraining approach. *CoRR*, abs/1907.11692, 2019.

Pan Lu, Liang Qiu, Jiaqi Chen, Tony Xia, Yizhou Zhao, Wei Zhang, Zhou Yu, Xiaodan Liang, and Song-Chun Zhu. Iconqa: A new benchmark for abstract diagram understanding and visual language reasoning. In *Proceedings of the Neural Information Processing Systems Track on Datasets and Benchmarks 1*, 2021.

Andrew Maas, Raymond E Daly, Peter T Pham, Dan Huang, Andrew Y Ng, and Christopher Potts. Learning word vectors for sentiment analysis. In *Proceedings of the Annual Meeting of the Association for Computational Linguistics*, pp. 142–150, 2011.

Adyasha Maharana, Prateek Yadav, and Mohit Bansal. $\mathbb{D}^2$ pruning: Message passing for balancing diversity and difficulty in data pruning. In *Proceedings of the International Conference on Learning Representations*, 2024.

Minesh Mathew, Dimosthenis Karatzas, and C.V. Jawahar. Docvqa: A dataset for vqa on document images. In *Proceedings of the IEEE/CVF Winter Conference on Applications of Computer Vision*, pp. 2200–2209, January 2021.

Minesh Mathew, Viraj Bagal, Rubèn Tito, Dimosthenis Karatzas, Ernest Valveny, and CV Jawahar. Infographicvqa. In *Proceedings of the IEEE/CVF Winter Conference on Applications of Computer Vision*, pp. 1697–1706, 2022.

Baharan Mirzasoleiman, Jeff A. Bilmes, and Jure Leskovec. Coresets for data-efficient training of machine learning models. In *Proceedings of the International conference on machine learning*, 2019.

Yixin Nie, Adina Williams, Emily Dinan, Mohit Bansal, Jason Weston, and Douwe Kiela. Adversarial nli: A new benchmark for natural language understanding. In *Proceedings of the Annual Meeting of the Association for Computational Linguistics*, pp. 4885–4901, 2020.

Feng Pan, Wei Wang, Anthony KH Tung, and Jiong Yang. Finding representative set from massive data. In *IEEE International Conference on Data Mining*, 2005.

Mansheej Paul, Surya Ganguli, and Gintare Karolina Dziugaite. Deep learning on a data diet: Finding important examples early in training. In *Proceedings of Advances in Neural Information Processing Systems*, pp. 20596–20607, 2021.

Geoff Pleiss, Tianyi Zhang, Ethan Elenberg, and Kilian Q Weinberger. Identifying mislabeled data using the area under the margin ranking. In *Proceedings of Advances in Neural Information Processing Systems*, pp. 17044–17056, 2020.

Ziheng Qin, K. Wang, Zangwei Zheng, Jianyang Gu, Xiang Peng, Daquan Zhou, and Yang You. Infobatch: Lossless training speed up by unbiased dynamic data pruning. In *Proceedings of the International Conference on Learning Representations*, 2023.

Alec Radford, Jong Wook Kim, Chris Hallacy, Aditya Ramesh, Gabriel Goh, Sandhini Agarwal, Girish Sastry, Amanda Askell, Pamela Mishkin, Jack Clark, Gretchen Krueger, and Ilya Sutskever. Learning transferable visual models from natural language supervision. In *Proceedings of the International Conference on Machine Learning*, pp. 8748–8763, 2021.

Sylvestre-Alvise Rebuffi, Alexander Kolesnikov, Georg Sperl, Christoph H Lampert, et al. Incremental classifier and representation learning. In *Proceedings of the IEEE/CVF Conference on Computer Vision and Pattern Recognition*, pp. 5533–5542, 2017.

Nils Reimers and Iryna Gurevych. Sentence-bert: Sentence embeddings using siamese bert-networks. In *Proceedings of the Conference on Empirical Methods in Natural Language Processing*, pp. 3980–3990, 2019.

Tanik Saikh, Tirthankar Ghosal, Amish Mittal, Asif Ekbal, and Pushpak Bhattacharyya. Scienceqa: a novel resource for question answering on scholarly articles. *International Journal on Digital Libraries*, 23(3):289–301, 2022.

Dustin Schwenk, Apoorv Khandelwal, Christopher Clark, Kenneth Marino, and Roozbeh Mottaghi. A-okvqa: A benchmark for visual question answering using world knowledge. In *Proceedings of European Conference on Computer Vision*, pp. 146–162, 2022.

Ozan Sener and Silvio Savarese. Active learning for convolutional neural networks: A core-set approach. In *Proceedings of the International Conference on Learning Representations*, 2018.

Burr Settles. Active learning literature survey. Technical Report 1648, University of Wisconsin–Madison, 2009.

Lloyd S. Shapley. Notes on the n-person game—ii: The value of an n-person game. Technical Report RM-670, RAND Corporation, 1951.

Karen Simonyan and Andrew Zisserman. Very deep convolutional networks for large-scale image recognition. In *Proceedings of the International Conference on Learning Representations*, 2015.

Ben Sorscher, Robert Geirhos, Shashank Shekhar, Surya Ganguli, and Ari Morcos. Beyond neural scaling laws: beating power law scaling via data pruning. In *Proceedings of Advances in Neural Information Processing Systems*, pp. 19523–19536, 2022.

Swabha Swayamdipta, Roy Schwartz, Nicholas Lourie, Yizhong Wang, Hannaneh Hajishirzi, Noah A Smith, and Yejin Choi. Dataset cartography: Mapping and diagnosing datasets with training dynamics. In *Proceedings of the Conference on Empirical Methods in Natural Language Processing*, pp. 9275–9293, 2020.

Michalis K Titsias, Jonathan Schwarz, Alexander G de G Matthews, Razvan Pascanu, and Yee Whye Teh. Functional regularisation for continual learning with gaussian processes. In *International Conference on Learning Representations*, 2020.

Mariya Toneva, Alessandro Sordoni, Remi Tachet des Combes, Adam Trischler, Yoshua Bengio, and Geoffrey J Gordon. An empirical study of example forgetting during deep neural network learning. In *Proceedings of the International Conference on Learning Representations*, 2019.

Laurens van der Maaten and Geoffrey Hinton. Visualizing data using t-sne. *Journal of Machine Learning Research*, 9(86):2579–2605, 2008.

Liyuan Wang, Xingxing Zhang, Hang Su, and Jun Zhu. A comprehensive survey of continual learning: theory, method and application. *IEEE Transactions on Pattern Analysis and Machine Intelligence*, 46(8):5362–5383, 2024.

Lai Wei, Zihao Jiang, Weiran Huang, and Lichao Sun. InstructionGPT-4: A 200-instruction paradigm for fine-tuning miniGPT-4. *CoRR*, abs/2308.12067, 2023.

Eyal Winter. *Chapter 53 The shapley value*, pp. 2025–2054. Elsevier, 2002.

Xiaobo Xia, Jiale Liu, Jun Yu, Xu Shen, Bo Han, and Tongliang Liu. Moderate coreset: A universal method of data selection for real-world data-efficient deep learning. In *Proceedings of the International Conference on Learning Representations*, 2023.

Shouxing Xiang, Xi Ye, Jiazhi Xia, Jing Wu, Yang Chen, and Shixia Liu. Interactive correction of mislabeled training data. In *Proceedings of IEEE Conference on Visual Analytics Science and Technology*, pp. 57–68, 2019.

Zhao Xu, Kai Yu, Volker Tresp, Xiaowei Xu, and Jizhi Wang. Representative sampling for text classification using support vector machines. In *Proceedings of Advances in Information Retrieval*, pp. 393–407, 2003.

Weikai Yang, Mengchen Liu, Zheng Wang, and Shixia Liu. Foundation models meet visualizations: Challenges and opportunities. *Computational Visual Media*, 10(3):399–424, 2024.

Jun Yuan, Shouxing Xiang, Jiazhi Xia, Lingyun Yu, and Shixia Liu. Evaluation of sampling methods for scatterplots. *IEEE Transactions on Visualization and Computer Graphics*, 27(2):1720–1730, 2021.

Friedemann Zenke, Ben Poole, and Surya Ganguli. Continual learning through synaptic intelligence. In *Proceedings of the International Conference on Machine Learning*, pp. 3987–3995, 2017.

Jianpeng Zhang, Hongchang Chen, Dingjiu Yu, Yulong Pei, and Yingjun Deng. Cluster-preserving sampling algorithm for large-scale graphs. *Science China Information Sciences*, 66(1):112103, 2023.

Shichao Zhang, Jiaye Li, Wenzhen Zhang, and Yongsong Qin. Hyper-class representation of data. *Neurocomputing*, 503:200–218, 2022.

Y. Zhao, H. Jiang, Q. Chen, Y. Qin, H. Xie, Y. Wu, S. Liu, Z. Zhou, J. Xia, and F. Zhou. Preserving minority structures in graph sampling. *IEEE Transactions on Visualization and Computer Graphics*, 27(2):1698–1708, 2021.

Haizhong Zheng, Rui Liu, Fan Lai, and Atul Prakash. Coverage-centric coreset selection for high pruning rates. In *Proceedings of the International Conference on Learning Representations*, 2022.

Dengyong Zhou, Jiayuan Huang, and Bernhard Schölkopf. Learning with hypergraphs: Clustering, classification, and embedding. In *Proceedings of Advances in Neural Information Processing Systems*, volume 19, 2006.

Deyao Zhu, Jun Chen, Xiaoqian Shen, Xiang Li, and Mohamed Elhoseiny. Minigpt-4: Enhancing vision-language understanding with advanced large language models. In *Proceedings of the International Conference on Learning Representations*, 2024.

He Zhu, Chong Zhang, Junjie Huang, Junran Wu, and Ke Xu. Hitin: Hierarchy-aware tree isomorphism network for hierarchical text classification. In *Proceedings of the Annual Meeting of the Association for Computational Linguistics*, pp. 7809–7821, 2023.

A Comparison of Encoding Tree Construction Methods

The construction of the encoding tree is an important step in our method. To the best of our knowledge, there are two methods for constructing the encoding tree: the one proposed by Li & Pan (2016) and the one proposed by Zhu et al. (2023). Both methods adopt the variations of the Huffman tree to construct the encoding tree. The key difference is that Zhu et al. (2023) further compresses the tree to a certain height to improve efficiency in subsequent processing. We assessed the two methods by calculating the Pearson correlation of the resulting node-level structural entropy. As shown in Table 5, the correlations on CIFAR10, CIFAR100, and ImageNet-1K exceed 0.99. Therefore, the choice of the construction method has a negligible effect on the sample selection results. In this paper, we employ the more recent method proposed by Zhu et al. (2023).

Table 5: Pearson correlation of the node-level structural entropy obtained from the two methods on CIFAR10, CIFAR100, and ImageNet-1K.

	CIAFR10	CIFAR100	ImageNet-1K
Correlation	0.996	0.999	0.992

B Proof of Proposition 1

We first present two lemmas essential for the proof of Proposition 1.

Lemma 1. *Let $G = (V, E, W)$ be an undirected, weighted graph and $\mathcal{T}$ be its encoding tree. Then the structural entropy $\mathcal{H}(G, \mathcal{T})$ can be written as:*

$$\mathcal{H}(G, \mathcal{T}) = \frac{1}{vol(V)} \left(2 \sum_{\langle u,v \rangle \in E} w_{u,v} \log vol(u \vee v) - \sum_{u \in V} d(u) \log d(u) \right),$$

where $w_{u,v}$ is the weight of edge $\langle u, v \rangle$, $u \vee v$ is the least common ancestor of node u and v in $\mathcal{T}$, and $d(u)$ is the weighted degree of node u.

Proof of Lemma 1. According to Eq. (1), we can derive that:

$$\begin{aligned} \mathcal{H}(G, \mathcal{T}) &= -\sum_{\alpha \in \mathcal{T}} \frac{g(\alpha)}{vol(V)} \log \frac{vol(\alpha)}{vol(\alpha^-)} \\ &= -\frac{1}{vol(V)} \sum_{\alpha \in \mathcal{T}} g(\alpha) \log \frac{vol(\alpha)}{vol(\alpha^-)} \\ &= \frac{1}{vol(V)} \sum_{\alpha \in \mathcal{T}} (g(\alpha) \log vol(\alpha^-) - g(\alpha) \log vol(\alpha)). \end{aligned} \tag{7}$$

For a node α with k children, the contribution of each child β_i to the summation is $g(\beta_i) \log vol(\alpha) - g(\beta_i) \log vol(\beta_i)$. The term $g(\beta_i) \log vol(\alpha)$ can be combined into $-g(\alpha) \log vol(\alpha)$ due to the shared $\log vol(\alpha)$ factor. By combining the terms with shared $\log vol(\cdot)$ factors, Eq. (7) can be rewritten as:

$$\mathcal{H}(G, \mathcal{T}) = \frac{1}{vol(V)} \left(\sum_{\alpha \text{ is non-leaf}} \left(\left(\sum_{\beta \in \text{children}(\alpha)} g(\beta) \right) - g(\alpha) \right) \log vol(\alpha) - \sum_{\alpha \text{ is leaf}} g(\alpha) \log vol(\alpha) \right). \tag{8}$$

Note that $\sum_{\beta \in \text{children}(\alpha)} g(\beta) - g(\alpha)$ represents the difference between the total weight of outer edges of α's children and the total weight of outer edges of α. This difference is precisely twice the total weights of edges between the communities represented by α's children. Furthermore, each edge

$\langle u, v\rangle$ in the graph contributes only to the node $\alpha = u \vee v$. Therefore, we can transform the first term into a sum over edges in the graph, yielding:

$$\mathcal{H}(G, \mathcal{T}) = \frac{1}{vol(V)} \left(2 \sum_{\langle u,v\rangle \in E} w_{u,v} \log vol(u \vee v) - \sum_{\alpha \text{ is leaf}} g(\alpha) \log vol(\alpha) \right). \tag{9}$$

The set of leaf nodes in the encoding tree corresponds to the set of nodes in the graph. Additionally, for a leaf node α and its correpsonding graph node u, we have $g(\alpha) = vol(\alpha) = d(u)$. We can conclude that:

$$\mathcal{H}(G, \mathcal{T}) = \frac{1}{vol(V)} \left(2 \sum_{\langle u,v\rangle \in E} w_{u,v} \log vol(u \vee v) - \sum_{u \in V} d(u) \log d(u) \right), \tag{10}$$

which proves the lemma.

Lemma 2 (Winter, 2002)**.** *Eq. (2) is equivalent to:*

$$\phi(u) = \frac{1}{|V|!} \sum_{\pi \in \Pi} \Big(\mathcal{H}(G[V_{\pi,u} \cup \{u\}], \mathcal{T}) - \mathcal{H}(G[V_{\pi,u}], \mathcal{T}) \Big), \tag{11}$$

where Π is the set of all permutations of nodes in V, and $V_{\pi,u}$ denotes the set of nodes preceding u in permutation π.

Based on the two lemmas, we develop a proof of Proposition 1.

Proof of Proposition 1. For brevity, we denote the subgraph $G[V_{\pi,u} \cup \{u\}]$ by $G^+_{\pi,u} = (V^+_{\pi,u}, E^+_{\pi,u}, W)$ and $G[V_{\pi,u}]$ by $G_{\pi,u} = (V_{\pi,u}, E_{\pi,u}, W)$. Lemma 1 gives:

$$\mathcal{H}(G^+_{\pi,u}, \mathcal{T}) = \frac{1}{vol(V)} (2 \sum_{\langle x,y\rangle \in E^+_{\pi,u}} w_{x,y} \log vol(x \vee y) - \sum_{x \in V^+_{\pi,u}} d(x) \log d(x)) \tag{12}$$

and

$$\mathcal{H}(G_{\pi,u}, \mathcal{T}) = \frac{1}{vol(V)} (2 \sum_{\langle x,y\rangle \in E_{\pi,u}} w_{x,y} \log vol(x \vee y) - \sum_{x \in V_{\pi,u}} d(x) \log d(x)). \tag{13}$$

Then

$$\begin{aligned} &\mathcal{H}(G^+_{\pi,u}, \mathcal{T}) - \mathcal{H}(G_{\pi,u}, \mathcal{T}) \\ &= \frac{1}{vol(V)} \Bigg(2(\sum_{\langle x,y\rangle \in E^+_{\pi,u}} w_{x,y} \log vol(x \vee y) - \sum_{\langle x,y\rangle \in E_{\pi,u}} w_{x,y} \log vol(x \vee y)) \\ &- (\sum_{x \in V^+_{\pi,u}} d(x) \log(x) - \sum_{x \in V_{\pi,u}} d(x) \log d(x)) \Bigg). \end{aligned} \tag{14}$$

Note that $V^+_{\pi,u} = V_{\pi,u} \cup \{u\}$ and $E^+_{\pi,u} = E_{\pi,u} \cup \{\langle u, v\rangle : v \in \mathcal{N}(u) \cap V_{\pi,u}\}$, where $\mathcal{N}(u)$ is the set of neighbors of u in G. Therefore,

$$\mathcal{H}(G^+_{\pi,u}, \mathcal{T}) - \mathcal{H}(G_{\pi,u}, \mathcal{T}) = \frac{1}{vol(V)} \left(2 \sum_{v \in \mathcal{N}(u) \cap V_{\pi,u}} w_{u,v} \log vol(u \vee v) - d(u) \log d(u) \right). \tag{15}$$

We can rewrite $\sum_{v\in\mathcal{N}(u)\cap V_{\pi,u}} \log vol(u\vee v)$ as $\sum_{v\in\mathcal{N}(u)} \mathbb{I}[v\in V_{\pi,u}]\log vol(u\vee v)$, where $\mathbb{I}$ is the indicator function. Then, the Shapley value in Eq. (11) can be rewritten as:

$$\begin{aligned}
\phi(u) &= \frac{1}{|V|!}\sum_{\pi\in\Pi}\Big(\mathcal{H}(G[V_{\pi,u}\cup\{u\}],\mathcal{T}) - \mathcal{H}(G[V_{\pi,u}],\mathcal{T})\Big) \\
&= \frac{1}{|V|!}\sum_{\pi\in\Pi}\left(\frac{1}{vol(V)}\left(2\sum_{v\in\mathcal{N}(u)}\mathbb{I}[v\in V_{\pi,u}]w_{u,v}\log vol(u\vee v) - d(u)\log d(u)\right)\right) \\
&= \frac{2}{vol(V)|V|!}\sum_{\pi\in\Pi}\sum_{v\in\mathcal{N}(u)}\mathbb{I}[v\in V_{\pi,u}]w_{u,v}\log vol(u\vee v) - \frac{1}{vol(V)}d(u)\log d(u) \\
&= \frac{2}{vol(V)|V|!}\sum_{v\in\mathcal{N}(u)} w_{u,v}\log vol(u\vee v)\sum_{\pi\in\Pi}\mathbb{I}[v\in V_{\pi,u}] - \frac{1}{vol(V)}d(u)\log d(u).
\end{aligned} \tag{16}$$

Note that $\sum_{\pi\in\Pi}\mathbb{I}[v\in V_{\pi,u}]$ is $\frac{|V|!}{2}$ since there are $\frac{|V|!}{2}$ permutations where v precedes u. Thus, we have:

$$\begin{aligned}
\phi(u) &= \frac{1}{vol(V)}\sum_{v\in\mathcal{N}(u)} w_{u,v}\log vol(u\vee v) - \frac{1}{vol(V)}d(u)\log d(u) \\
&= \frac{1}{vol(V)}\left(\sum_{v\in\mathcal{N}(u)} w_{u,v}\log vol(\alpha_{u\vee v}) - d(u)\log d(u)\right) \\
&= \frac{1}{vol(V)}\left(\sum_{\langle u,v\rangle\in E} w_{u,v}\log vol(\alpha_{u\vee v}) - d(u)\log d(u)\right),
\end{aligned} \tag{17}$$

which proves the proposition.

C Theoretical Analysis of Node-Level Structural Entropy

C.1 Node-Level Structural Entropy and Sample Coverage

In this section, we prove that node-level structural entropy serves as a lower bound for the sample coverage. Following previous work (Zheng et al., 2022), we assume that the dataset $S=\{\mathbf{x}_i,y_i\}$ contains n i.i.d. samples drawn from an underlying distribution P_μ with probability measure μ. We discuss a certain sample u's ability to cover the entire distribution, i.e., how well the sample can cover the entire distribution. The sample coverage of a sample $\mathbf{u}$ can be quantified by the coverage of the entire distribution by a ball $B(\mathbf{u},r)$ centered at $\mathbf{u}$ with radius r (Zheng et al., 2022):

$$P(u,r) = \int_{B(u,r)} \mathrm{d}\mu(x).$$

When r is fixed, the larger $P(u,r)$ is, the better sample covers the distribution. Directly calculating $P(u,r)$ is difficult because we do not know the underlying distribution P_μ. We next prove that node-level structural entropy serves as a lower bound for the sample coverage.

We assume that the edge weights are in the range $[L,R]$, where $R>L>0$. Consider a node u connected to k other nodes $\{v_1,v_2,\ldots,v_k\}$ with edge weights $\{w_1,w_2,\ldots,w_k\}$. In the BFS tree rooted at u, let the total vol of the subtrees of $v_1,v_2\ldots,v_k$ be $vol_1,vol_2,\ldots,vol_k$. From the perspective of u, the calculation of $S_e(u)$ is as follows: $vol(u)$ is initially set to 0; For each node v_i connected to u, add vol_i of v_i to $vol(u)$, and then add $w_i vol(u)$ to $S_e(u)$. If the nodes are connected in the oreder $\{\pi_1,\pi_2,\ldots,\pi_k\}$, the results is:

$$S_e(u) = \sum_{i=1}^{k} w_{\pi_i}\log(vol_{\pi_1}+vol_{\pi_2}+...vol_{\pi_k}).$$

In practice, the nodes are connected in a specific order to minimize $S_e(u)$. Consequently, $S_e(u)$ is less than or equal to values obtained in any other order. Consider the order in which nodes are connected from the smallest w_i to the largest w_i. We derive that:

$$\begin{aligned}
S_e(u) &\leq \sum_{i=1}^{k} w_{\pi_i} \log(vol_{\pi_1} + vol_{\pi_2} + ...vol_{\pi_k}) \\
&\leq \left(\sum_{i=1}^{k} w_i\right) \log \sum_{i=1}^{k} \left(\frac{w_{\pi_k}}{\sum_{i=1}^{k} w_i}(vol_{\pi_1} + ... + vol_{\pi_k})\right) \text{(Jensen's Inequality)} \\
&= \left(\sum_{i=1}^{k} w_i\right) \log \sum_{i=1}^{k} (vol_{\pi_k}(w_{\pi_1} + w_{\pi_2} + ...w_{\pi_k}) / \sum_{i=1}^{k} w_i) \\
&\leq kR \log \sum_{i=1}^{k} (vol_{\pi_k}(w_{\pi_1} + w_{\pi_2} + ...w_{\pi_k}) / \sum_{i=1}^{k} w_i) \\
&\leq kR \log \sum_{i=1}^{k} (kvol_{\pi_k} w_{\pi_k} / \sum_{i=1}^{k} w_i)
\end{aligned} \tag{18}$$

Because $vol_{\pi_k} \in [kLn_{\pi_k}, kRn_{\pi_k}]$, where n_{π_k} is the number of nodes in the subtree of v_{π_k}. So we have:

$$S_e(u) \leq kR \log(k^2 R \sum_{i=1}^{k} n_{\pi_i} w_{\pi_i} / \sum_{i=1}^{k} w_i)$$

Assume that all nodes in the subtree of v_i are in $B(v_i, r^*)$. Then we have:

$$\mathbb{E}[n_{i_k}] = n \int_{B(v_i, r^*)} \mathrm{d}\mu = nP(v_i, r^*)$$

which can then lead to:

$$\begin{aligned}
\mathbb{E}[S_e(u)] &\leq \mathbb{E}[kR \log \left(k^2 R (\sum_{i=1}^{k} n_{\pi_i} w_{\pi_i} / \sum_{i=1}^{k} w_i)\right)] \\
&\leq kR \log \mathbb{E}\left[k^2 R \left(\sum_{i=1}^{k} n_{\pi_i} w_{\pi_i} / \sum_{i=1}^{k} w_i\right)\right] \text{(Jensen's Inequality)} \\
&= kR \log \mathbb{E}\left[nk^2 R \left(\sum P(v_{\pi_i}, r^*) w_{\pi_i} / \sum_{i=1}^{k} w_i\right)\right]
\end{aligned} \tag{19}$$

Since

$$\sum_{i=1}^{k} P(v_{\pi_i}, r^*) w_{\pi_i} / \sum_{i=1}^{k} w_i = \hat{P}(u, r)$$

is actually the Nadaraya–Watson estimator of $P(u, r^*)$, we have:

$$\mathbb{E}[S_e(u)] \leq KR \log \mathbb{E}\left[nK^2 R \hat{P}(u, r)\right]$$

Thus, the following theorem is obtained:

Theorem 1. *For $r > r^*$, $S_e(u)$ ensures an lower-bound of the Nadaraya–Watson estimator $\hat{P}(u, r^*)$ of $P(u, r^*)$ with inequality:*

$$\frac{1}{nK^2 R} \exp\left(\frac{1}{KR} \mathbb{E}[S_e(u)]\right) \leq \mathbb{E}[\hat{P}(u, r)] \approx \mathbb{E}[P(u, r)]$$

where r^* is a constant related to the distribution P_μ and the location of u in the metric space.

Theorem 1 shows the correlation between $S_e(u)$ and $P(u, r)$. For a certain sample u, a larger $S_e(u)$ guarantees a stronger sample coverage.

C.2 Sample Coverage and Model Performance

Previous work (Zheng et al., 2022) has demonstrated that a better distribution coverage brings a lower empirical loss, as depicted by the following theorem:

Theorem 2. Zheng et al. (2022) *Given n i.i.d. samples drawn from P_μ as $S = \{\boldsymbol{x_i}, y_i\}_{i\in[n]}$ where $\boldsymbol{x_i} \in X = \mathbb{R}^d$ is the feature representation of example i and $y_i \in [C]$ is the class label for example i, a coreset S' which is a p-partial r-cover for P_μ on the feature space X, and an $\epsilon > 1 - p$, if the loss function $l(\cdot, y, w)$ is λ_l -Lipschitz continuous for all y, w and bounded by L, the class-specific regression function $\eta_c(x) = p(y = c|\boldsymbol{x})$ is λ_η-Lipschitz for all c, and $l(\boldsymbol{x}, y; h_{S'}) = 0$, $\forall(\boldsymbol{x}, y) \in S'$, then with probability at least $1 - \epsilon$:*

$$\left| \frac{1}{n} \sum_{\boldsymbol{x},y\in S} l(x, y; h_{S'}) \right| \leq r(\lambda_l + \lambda_\eta LC) + L\sqrt{\frac{\log \frac{p}{p+\epsilon-1}}{2n}} \tag{20}$$

Theorem 2 suggests that better sample coverage results in a tighter bound on the empirical loss for the entire set. Given the relationship between $S_e(u)$ and sample coverage, selecting samples with high node-level structural entropy effectively enhances model performance.

D Dataset Statistics and Detailed Experimental Setting

D.1 Supervised Learning

Image classification. The CIFAR10 and CIFAR100 datasets each consist of $50,000$ images of 32×32 pixels for the training set, with an additional $10,000$ images for testing. CIFAR10 includes 10 distinct classes, while CIFAR100 includes 100 classes. The ImageNet-1K dataset includes $1,281,167$ images across $1,000$ real-world classes for training, along with $50,000$ images for validation. Following common practice (Maharana et al., 2024), we trained ResNet-18 for 200 epochs on CIFAR10 and CIFAR100, and ResNet-34 for 60 epochs on ImageNet-1K. The batch size is set to 64. We use an SGD optimizer with an initial learning rate of 0.1, momentum of 0.9, and weight decay of 0.0002. We use a cosine annealing learning rate scheduler with a minimum learning rate of 0.0001.

Text classification. The ANLI dataset is a natural language inference dataset created through multiple rounds of iterative human-and-model-in-the-loop adversarial procedures. We utilize the data from the final round, which consists of $100,459$ training samples and $1,200$ test samples. Following previous work (Maharana et al., 2024), we fine-tune the RoBERTa model for $10,000$ iterations with a batch size of 16. We use the SGD optimizer with an initial learning rate of 0.1, momentum of 0.9, and weight decay of 0.0005. We use a cosine annealing scheduler with a minimum learning rate of 0.0001.

The IMDB Review dataset contains $25,000$ movie reviews each in the training and test splits, with each review labeled by sentiment (positive/negative). Following previous work (Maharana et al., 2024), we randomly select $2,000$ samples from the original training set due to the excessive samples in it, and use the original test set for evaluation. We fine-tune the RoBERTa model for 500 iterations with a batch size of 16. The optimizer and scheduler settings are the same as that for the ANLI dataset.

Object detection. We train the model using the combined trainval sets of PASCAL VOC 2007 and 2012, which include $16,551$ images and $40,058$ objects across 20 categories. The model is evaluated on the PASCAL VOC 2007 test set, which comprises $4,952$ images and $12,032$ objects. We train SSD (Liu et al., 2016) with VGG-16 (Simonyan & Zisserman, 2015) backbone from scratch for 80 epochs with a batch size of 64. We use an SGD optimizer with a learning rate of 0.001, momentum of 0.9, and weight decay of 0.0005. The learning rate follows a linear warm-up strategy for the first 8 epochs and is then reduced by a factor of 10 at epochs 50 and 70.

Visual question answering. The CC SBU Align dataset contains $3,439$ high-quality, aligned image-text pairs for the fine-tuning stage (stage 2) of Mini-GPT4 (Zhu et al., 2024). The visual question answering datasets used for validation test the model's abilities in various aspects, including logical reasoning, visual reasoning, knowledge retention, and abstract understanding. We use the same setting as the second-stage fine-tuning for Mini-GPT4 (Zhu et al., 2024). We fine-tune MiniGPT-4

for 400 iterations with a batch size of 12. We use an SGD optimizer with an initial learning rate of 0.00003, momentum of 0.9, and weight decay of 0.05. We use a cosine annealing scheduler with a minimum learning rate of 0.00001.

D.2 ACTIVE LEARNING

We use the same setting as training on ImageNet-1K in Appendix D.1.

D.3 CONTINUAL LEARNING

For continual learning, we follow Borsos et al. (2020) for experiments on Permuted MNIST, Split MNIST, and Split CIFAR10, and follow Hao et al. (2024) for experiments on Split CIFAR100 and Split Tiny-ImageNet. We use increasingly complex models as dataset complexity grows: a two-layer MLP for Permuted MNIST, a four-layer CNN for Split MNIST, ResNet-18 for Split CIFAR10, and ResNet-18 with multi-head output (Zenke et al., 2017) for Split CIFAR100 and Split Tiny-ImageNet. For each task, we first randomly select $\mathcal{M}$ samples from all available samples. Then, we train the model on these samples for E epochs with a batch size of $\mathcal{B}$. During each training iteration, all replay samples are used with a weight of λ. The initial learning rate is set to lr_t for the first task and decays by a factor of η for each task. All hyperparameters, except λ, are fixed for all baselines and our method. The value of λ is determined through a grid search over $\{0.01, 0.1, 1, 10, 100, 1000\}$. Table 6 shows the fixed hyperparameters for different datasets. Table 7 shows the optimal λ for all baselines and our method.

Table 6: Training hyperparameters for continual learning.

Hyperparameters	Permuted MNIST	Split MNIST	Split CIFAR10	Split CIFAR100	Split Tiny-ImageNet
$\mathcal{M}$	1000	1000	1000	2500	5000
Optimizer	Adam	Adam	Adam	SGD	SGD
E	400	400	400	1	1
$\mathcal{B}$	256	256	256	10	20
lr_t	0.0005	0.0005	0.0005	0.15	0.20
η	1	1	1	0.875	0.875

Table 7: Optimal replay sample weight λ in continual learning.

Dataset	Permuted MNIST		Split MNIST		Split CIFAR10		Split CIFAR100		Split Tiny-ImageNet	
Memory size	100	200	100	200	100	200	100	200	100	200
Random	0.01	0.01	100	100	0.01	0.01	0.01	0.01	0.01	0.01
Moderate	0.01	0.01	100	100	0.1	0.1	0.01	0.01	0.01	0.01
CCS	0.01	0.01	1000	100	0.01	0.01	0.01	0.01	0.01	0.01
$\mathbb{D}^2$ Pruning	0.01	0.01	10	100	0.1	0.01	0.01	0.01	0.01	0.01
GraphCut	0.01	0.01	100	1	0.01	0.1	0.01	0.1	1	0.1
Entropy	0.01	0.01	1000	100	0.01	0.01	0.01	0.01	0.01	0.01
Forgetting	0.01	0.01	100	10	0.1	0.1	0.01	0.01	0.01	0.1
EL2N	0.01	0.01	100	100	0.01	0.1	0.01	0.01	0.01	0.01
AUM	0.01	0.01	100	100	10	1	0.01	0.01	0.01	0.01
Variance	0.01	0.01	1000	1000	0.01	0.01	0.01	0.01	0.01	0.01
iCaRL	0.01	0.1	100	100	1	1	0.01	0.01	0.1	0.1
Greedy Coreset	0.01	0.01	100	10	0.01	0.01	0.01	0.1	0.01	0.01
BCSR	0.01	0.01	100	10	0.01	0.01	0.01	0.01	0.01	0.01
SES (Ours)	0.01	0.1	100	100	1	1	0.01	0.1	0.01	0.1

E SELECTION HYPERPARAMETER SETTINGS

E.1 SELECTION HYPERPARAMETERS

We conducted a grid search to optimize three hyperparameters: the number of neighbors k for constructing the kNN graph, the cutoff ratio β to remove the most difficult samples, and the imbalance factor γ to maintain the balance between different classes.

Selecting an appropriate value of k is crucial as it can significantly affect the quality of the sample graph and thus affect the selection result. If k is too small, the graph becomes too sparse, making the selection sensitive to noise and outliers. If k is too large, the graph will be too dense and contain many edges connecting irrelevant neighbors, making it hard to identify the most important samples in the dataset. Thus, the choice of k must strike a balance to preserve meaningful structures without introducing noise or irrelevant information.

Inspired by Zheng et al. (2022), we also search the hard cutoff ratio β that removes β of the most difficult samples because they are usually outliers and contain noisy samples in the dataset. In addition, we also allow negative β during the grid search, which indicates that we will remove $|\beta|$ of the easiest samples to focus on difficult samples, which has been adopted by Sorscher et al. (2022).

Maintaining a balanced distribution of samples from different classes is also beneficial for model training. A common strategy is to enforce strict class balance (Guo et al., 2022) by selecting an equal number of samples from each class. However, this overlooks the difference between classes, where some may be more easily confused with others and require more samples to distinguish. To address this, we introduce an imbalance factor $\gamma > 1$, which allows for the selection of up to $n\dot{\gamma}$ samples per class, rather than a strict count of n. This adjustment provides flexibility in addressing class-specific complexities. In the active learning scenario, we treat the k-means clusters as the classes for balancing.

E.2 PRELIMINARY EXPERIMENTS ON K

As k decides the sample graph and the range of possible k is large, we conduct preliminary experiments on CIFAR10, CIFAR100, and ImageNet-1k to determine a candidate range where the structure of the sample graph is effectively preserved by the kNN-graph.

Spectral clustering is an effective method for revealing the underlying structural features of a graph. Therefore, we use the spectral clustering results to evaluate the choice of k in the preliminary experiments. First, we perform spectral clustering on the kNN-graph. Based on the spectral clustering results, we measure the structure preservation of the kNN-graph using both external and internal metrics. The external metrics measure the consistency of the clustering results with the ground truth labels of samples. We use the accuracy, the Rand Index, and the mutual information as the external metrics. The internal metrics assess the quality of clustering by evaluating the compactness and separation of clusters. We use the Silhouette Score and the Davis-Bouldin Index as the internal metrics.

Directly applying spectral clustering to large-scale datasets is unsuitable due to its high complexity of $O(n^3)$, where n is the number of samples in the dataset. To address this, we use growing neural gas (Fritzke, 1995) to generate a reduced graph with fewer nodes. The key feature of this method is the preservation of the topology of the kNN-graph. Specifically, this method generates neurons representing the sample distribution of the kNN-graph. Then, it integrates the edges in the kNN-graph into the neuron connections, resulting in a sparse, topology-preserving graph. We apply spectral clustering to this reduced graph to accelerate the evaluation of the choice of k.

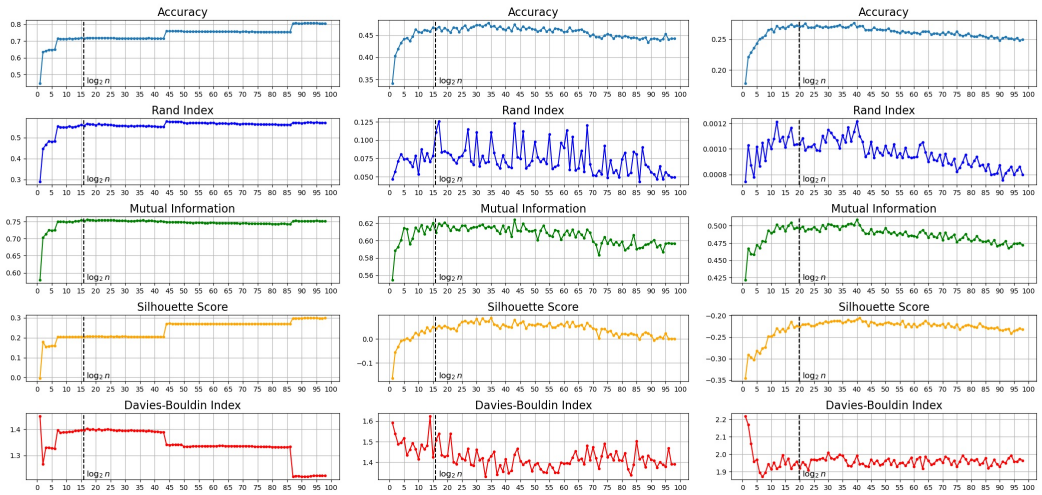

(a) CIFAR10 (b) CIFAR100 (c) ImageNet-1K

Figure 5: Results for the preliminary experiments on: (a) CIFAR10; (b) CIFAR100; (c) ImageNet-1K. An increase in the accuracy, the Rand Index, the mutual information, and the Silhouette Score, as well as a decrease in the Davis-Bouldin Index, indicates better structure preservation.

In the preliminary experiments, we test k in $\{1, 2, \ldots, 100\}$ on CIFAR10, CIFAR100, and ImageNet-1K. Fig. 5 presents the results. As the value of k increases, the performance metrics initially improve, then stabilize, and may eventually decline. This suggests that the first few nearest neighbors effectively capture the structure of the original graph, while including too many neighbors may lead to underfitting due to edges connecting vastly different nodes. We discover that the metrics begin to stabilize around $\log_2 n$, where n is the number of samples in the dataset. Thus, we focus our grid search for k values near $\log_2 n$.

E.3 Grid Search Results

For all experiments, we search β in $\{-1, -0.95, \ldots, -0.05, 0, 0.05, \ldots, 0.95, 1\}$ and γ in $\{1, 1.05, \ldots, 1.5\}$. For CIFAR10 and CIFAR100, we search k in $\{10, 11, \ldots, 30\}$. For ImageNet-1K, we search it only in $\{20, 25\}$ due to computational costs. To save computational costs, we set k to around $\log_2 n$ for experiments on other datasets. With this choice, the kNN graph has $O(n \log_2 n)$ edges, resulting in a Shapley value calculation time complexity of $O(n \log_2 n)$. This complexity is comparable to sorting and is lower than or equal to that of typical sample selection methods, which is at least $O(n \log_2 n)$ when sorting is required and $O(n^2)$ when an enumeration of all pairs of samples is required. For extremely large datasets (e.g. DataComp (Gadre et al., 2024) with billions of samples) where this complexity becomes impractical, a potential solution is to split the dataset into bins before selection. Determining an optimal splitting method remains an open question and a promising direction for future research. We evaluate every possible combination of the hyperparameters. Table 8 presents the optimal hyperparameters for supervised learning and active learning. Table 9 presents the optimal hyperparameters for continual learning.

Table 8: Optimal hyperparameters of our method in supervised learning and active learning. The three numbers in each tuple refer to the number of neighbors k, the cutoff ratio β, and the imbalance factor γ, respectively.

Sampling rate	CIFAR10	CIFAR100	ImageNet-1K	ANLI	IMDB Review	PASCAL VOC	VQA	ImageNet-1K (active learning)
1%	(17,0.75,1.05)	(14,0.85,1.2)	(20,0.9,1.3)	(15,0.35,1.05)	(10,0.7,1.2)	(15,0.7,/)	(10,0.15,/)	(25,0.25,1.05)
2%	(14,0.7,1.1)	(10,0.85,1.15)	(25,0.75,1.2)	(15,0.3,1.05)	(10,0.85,1.1)	(15,0.7,/)	(10,0.1,/)	(25,0.2,1.45)
5%	(19,0.6,1.05)	(21,0.8,1.2)	(25,0.65,1.2)	(15,0.25,1.05)	(10,0.5,1.0)	(15,0.5,/)	(10,0.1,/)	(25,0.4,1.35)
10%	(11,0.35,1.1)	(19,0.6,1.1)	(25,0.4,1.15)	(15,0.3,1.15)	(10,0.4,1.05)	(15,0.35,/)	(10,0.15,/)	(25,0.45,1.05)
20%	(13,0.2,1.0)	(15,0.45,1.15)	(25,0.3,1.1)	(15,0.0,1.05)	(10,0.3,1.1)	(15,0.1,/)	(10,0.15,/)	(25,0.35,1.15)
50%	(15,-0.15,1.0)	(15,0.15,1.0)	(20,0.05,1.05)	(15,0.0,1.1)	(10,0.05,1.05)	(15,0.15,/)	(10,0.1,/)	(25,0.0,1.1)
70%	(24,0.0,1.0)	(18,0.1,1.0)	(20,0.0,1.0)	(15,0.0,1.2)	(10,0.05,1.0)	(15,0.05,/)	(10,0.0,/)	(25,0.0,1.15)

Table 9: Optimal hyperparameters of our method in continual learning. The three numbers in each tuple refer to the number of neighbors k, the cutoff ratio β, and the imbalance factor γ, respectively.

Memory size	Permuted MNIST	Split MNIST	Split CIFAR10	Split CIFAR100	Split Tiny-ImageNet
100	(15,-0.15,1.25)	(15,0.7,1.5)	(15,-0.35,1.0)	(15,-0.95,1.0)	(15,-0.15,1.0)
200	(15,-0.45,1.5)	(15,0.75,1.1)	(15,-0.7,1.1)	(15,-0.85,1.0)	(15,-0.9,1.0)

F Detailed Experimental Results

F.1 Superivised Learning

We present detailed experimental results for supervised learning from Table 10 to 16. Our method consistently performs better than baselines across all tasks and sampling rates. Meanwhile, several factors prevent us from achieving more significant improvements over the baselines in certain settings:

- In high-sampling-rate settings for simple datasets, such as the 70% setting for CIFAR10, all methods perform closely to using the entire training set, leaving little room for improvement.
- In low-sampling-rate settings for challenging datasets, such as the 1% setting for ImageNet-1K, the performance of all methods is limited due to the insufficient number of samples per class.
- In scenarios where models are fine-tuned from pretrained weights, the knowledge within these models anchors the performance at a certain level, leading to similar performance across all methods.

Despite these factors, our method achieves significant improvement in many settings. For example, it achieves a 5.52% increase in accuracy when selecting 2% of the samples from ImageNet-1K.

Table 10: Results on image classification (CIFAR10). The best one is **bold**, and the runner-up is underlined.

Dataset	**CIFAR10 (100%:95.49)**						
Sampling rate	**70%**	**50%**	**20%**	**10%**	**5%**	**2%**	**1%**
Random	94.29 ± 0.08	92.33 ± 0.15	84.17 ± 0.62	71.95 ± 1.50	59.88 ± 2.45	45.51 ± 1.68	35.44 ± 1.49
Moderate	94.04 ± 0.26	92.36 ± 0.17	80.96 ± 2.56	63.91 ± 1.56	49.94 ± 0.70	32.00 ± 2.11	26.18 ± 1.94
CCS	94.23 ± 0.35	93.83 ± 0.15	83.85 ± 1.10	75.56 ± 2.39	65.89 ± 1.04	49.02 ± 1.35	40.24 ± 0.96
$\mathbb{D}^2$ Pruning	93.17 ± 0.11	93.70 ± 0.20	86.83 ± 0.48	76.56 ± 1.14	65.12 ± 0.88	45.44 ± 1.75	39.03 ± 1.69
GraphCut	94.38 ± 0.20	92.43 ± 0.23	81.98 ± 0.48	69.29 ± 0.57	59.36 ± 2.43	46.93 ± 2.21	39.68 ± 1.15
Entropy	94.13 ± 0.30	92.39 ± 0.40	75.34 ± 4.32	60.66 ± 6.23	46.17 ± 5.96	35.85 ± 4.33	29.28 ± 4.29
Forgetting	94.76 ± 0.38	94.34 ± 0.17	57.72 ± 1.17	35.21 ± 0.87	30.87 ± 0.57	27.22 ± 0.49	23.62 ± 0.74
EL2N	94.75 ± 0.32	94.10 ± 0.45	46.41 ± 4.84	22.40 ± 0.62	15.66 ± 0.18	13.05 ± 0.20	12.75 ± 0.56
AUM	94.90 ± 0.17	94.38 ± 0.20	51.98 ± 1.32	30.56 ± 0.42	22.92 ± 0.38	18.10 ± 0.47	14.50 ± 1.35
Variance	90.45 ± 0.09	85.81 ± 0.39	64.90 ± 0.53	53.64 ± 1.02	44.45 ± 0.77	36.61 ± 0.70	31.46 ± 0.92
***k*-means**	93.87 ± 0.33	93.19 ± 0.36	83.68 ± 0.94	72.46 ± 0.51	62.68 ± 1.12	48.35 ± 2.29	38.73 ± 0.87
***k*-DPP**	93.84 ± 0.10	92.72 ± 0.18	84.09 ± 1.21	74.62 ± 0.40	61.95 ± 4.87	46.58 ± 1.76	35.16 ± 2.92
SES (Ours)	$\mathbf{95.01 \pm 0.08}$	$\mathbf{94.50 \pm 0.05}$	$\mathbf{88.31 \pm 0.13}$	$\mathbf{80.24 \pm 0.72}$	$\mathbf{69.82 \pm 0.84}$	$\mathbf{54.78 \pm 1.36}$	$\mathbf{45.25 \pm 0.81}$

Table 11: Results on image classification (CIFAR100). The best one is **bold**, and the runner-up is underlined.

Dataset	CIFAR100 (100%:77.90)						
Sampling rate	70%	50%	20%	10%	5%	2%	1%
Random	74.72 ± 0.16	70.51 ± 0.43	52.29 ± 2.32	37.38 ± 0.80	23.03 ± 0.48	13.38 ± 0.36	8.57 ± 0.65
Moderate	74.61 ± 0.10	69.95 ± 0.32	49.37 ± 0.58	30.53 ± 1.44	17.68 ± 0.50	9.28 ± 0.34	5.97 ± 0.35
CCS	76.10 ± 0.29	73.12 ± 0.21	58.39 ± 1.04	44.92 ± 1.81	28.68 ± 0.99	15.93 ± 0.62	10.28 ± 0.54
$\mathbb{D}^2$ Pruning	76.00 ± 0.56	74.45 ± 0.36	59.08 ± 0.53	44.78 ± 0.78	26.68 ± 0.85	13.90 ± 0.66	9.61 ± 0.44
GraphCut	76.64 ± 0.13	68.79 ± 0.35	25.08 ± 1.10	16.46 ± 0.35	10.78 ± 0.52	7.84 ± 0.35	5.94 ± 0.16
Entropy	76.81 ± 0.12	62.52 ± 0.26	33.28 ± 7.01	21.85 ± 7.11	13.90 ± 4.75	8.31 ± 2.69	5.30 ± 1.71
Forgetting	76.64 ± 0.13	68.75 ± 0.34	25.17 ± 1.12	16.45 ± 0.37	10.70 ± 0.49	7.82 ± 0.37	5.90 ± 0.09
EL2N	76.15 ± 0.50	66.19 ± 0.48	14.85 ± 0.43	7.50 ± 0.27	5.28 ± 0.12	3.83 ± 0.07	3.17 ± 0.14
AUM	76.84 ± 0.40	67.81 ± 0.59	16.66 ± 0.90	8.54 ± 0.10	5.60 ± 0.18	4.35 ± 0.17	3.56 ± 0.10
Variance	73.69 ± 0.14	68.42 ± 0.16	49.60 ± 0.28	34.63 ± 0.42	22.70 ± 0.35	13.71 ± 0.38	9.18 ± 0.52
***k*-means**	74.93 ± 0.12	72.86 ± 0.17	56.86 ± 0.88	42.69 ± 0.52	26.39 ± 0.73	14.92 ± 0.75	8.90 ± 0.31
***k*-DPP**	75.34 ± 0.45	73.16 ± 0.45	56.88 ± 1.01	42.09 ± 0.41	26.55 ± 0.9	14.31 ± 0.33	8.23 ± 0.27
SES (Ours)	$\mathbf{77.23 \pm 0.10}$	$\mathbf{74.63 \pm 0.17}$	$\mathbf{61.52 \pm 0.76}$	$\mathbf{48.02 \pm 0.98}$	$\mathbf{33.39 \pm 0.27}$	$\mathbf{19.68 \pm 0.51}$	$\mathbf{14.16 \pm 0.48}$

Table 12: Results on image classification (ImageNet-1K). The best one is **bold**, and the runner-up is underlined.

Dataset	ImageNet-1K (100%:73.63)						
Sampling rate	70%	50%	20%	10%	5%	2%	1%
Random	71.63 ± 0.12	69.26 ± 0.17	58.90 ± 0.12	47.10 ± 0.26	34.04 ± 0.42	16.56 ± 0.11	5.50 ± 0.28
Moderate	71.33 ± 0.04	68.72 ± 0.07	55.23 ± 0.27	40.97 ± 0.18	25.75 ± 0.16	11.33 ± 0.31	4.52 ± 0.24
CCS	70.74 ± 0.09	69.23 ± 0.09	60.04 ± 0.95	50.41 ± 0.11	36.92 ± 1.62	19.92 ± 1.36	9.43 ± 0.31
$\mathbb{D}^2$ Pruning	71.29 ± 0.07	70.32 ± 0.05	58.91 ± 0.04	50.81 ± 0.24	37.12 ± 0.09	18.97 ± 0.05	11.23 ± 0.26
GraphCut	68.91 ± 0.05	68.72 ± 0.07	55.28 ± 0.17	44.79 ± 0.06	33.54 ± 0.12	20.07 ± 0.21	11.49 ± 0.12
Entropy	70.93 ± 0.74	69.21 ± 0.12	54.76 ± 0.16	38.46 ± 0.34	22.78 ± 0.73	7.01 ± 0.24	1.95 ± 0.15
Forgetting	70.57 ± 0.04	70.46 ± 0.10	60.77 ± 0.02	48.73 ± 0.12	33.86 ± 0.15	15.13 ± 0.23	5.66 ± 0.30
EL2N	71.68 ± 0.04	65.98 ± 0.12	31.90 ± 3.64	12.57 ± 0.11	6.50 ± 0.36	3.25 ± 0.13	1.90 ± 0.09
AUM	69.94 ± 0.30	65.36 ± 0.11	21.91 ± 0.13	10.50 ± 0.19	6.42 ± 0.07	3.58 ± 0.07	2.24 ± 0.05
Variance	70.12 ± 0.09	66.09 ± 0.01	35.15 ± 0.09	13.85 ± 0.02	7.13 ± 0.05	4.72 ± 0.02	1.81 ± 0.06
***k*-means**	70.33 ± 0.07	69.47 ± 0.11	59.23 ± 0.22	48.12 ± 0.21	35.51 ± 0.13	18.67 ± 0.08	9.65 ± 0.33
***k*-DPP**	70.84 ± 0.09	69.85 ± 0.14	59.92 ± 0.33	46.10 ± 0.33	34.41 ± 0.07	16.33 ± 0.15	7.49 ± 0.17
SES (Ours)	$\mathbf{72.80 \pm 0.03}$	$\mathbf{71.05 \pm 0.09}$	$\mathbf{63.24 \pm 0.06}$	$\mathbf{53.59 \pm 0.09}$	$\mathbf{41.88 \pm 0.13}$	$\mathbf{25.59 \pm 0.17}$	$\mathbf{13.43 \pm 0.37}$

Table 13: Results on text classification (ANLI). The best one is **bold**, and the runner-up is underlined.

Dataset	ANLI (100%:49.25)						
Sampling rate	70%	50%	20%	10%	5%	2%	1%
Random	47.08 ± 0.26	45.20 ± 0.50	42.13 ± 0.54	39.52 ± 0.93	38.82 ± 1.06	37.50 ± 1.29	35.96 ± 1.04
Moderate	46.84 ± 0.31	45.11 ± 0.39	41.95 ± 0.33	40.16 ± 0.85	38.99 ± 0.45	35.83 ± 1.39	33.91 ± 0.62
CCS	46.56 ± 0.23	45.92 ± 0.70	41.67 ± 1.39	41.63 ± 0.97	40.33 ± 0.65	37.41 ± 0.05	36.82 ± 0.49
$\mathbb{D}^2$ Pruning	48.56 ± 1.22	47.49 ± 0.17	42.77 ± 0.36	41.43 ± 0.24	40.34 ± 0.07	37.92 ± 1.44	36.29 ± 0.59
GraphCut	46.14 ± 0.67	44.53 ± 0.55	42.12 ± 0.66	39.86 ± 0.27	38.15 ± 0.74	35.44 ± 0.80	34.02 ± 0.61
Entropy	46.32 ± 1.11	45.53 ± 0.44	41.45 ± 0.33	39.67 ± 0.28	38.54 ± 0.66	36.69 ± 0.53	36.40 ± 0.19
Forgetting	48.73 ± 0.35	42.29 ± 0.17	39.82 ± 0.16	38.37 ± 0.60	35.95 ± 0.33	35.78 ± 0.42	35.03 ± 0.77
EL2N	48.70 ± 0.65	47.85 ± 0.98	43.14 ± 1.68	39.63 ± 2.20	37.52 ± 1.05	34.33 ± 1.15	34.27 ± 0.42
AUM	47.86 ± 0.27	47.58 ± 0.37	43.57 ± 0.71	40.02 ± 1.51	34.66 ± 0.73	34.16 ± 0.12	33.62 ± 0.12
Variance	47.97 ± 0.30	47.87 ± 0.56	40.70 ± 0.16	38.75 ± 0.62	33.52 ± 0.03	33.50 ± 0.03	33.17 ± 0.12
***k*-means**	46.48 ± 0.24	46.52 ± 1.06	42.42 ± 0.72	40.57 ± 0.65	39.89 ± 0.10	36.74 ± 0.29	36.11 ± 0.40
***k*-DPP**	47.74 ± 0.07	47.02 ± 0.02	43.44 ± 0.59	40.98 ± 0.46	40.12 ± 0.26	37.44 ± 0.11	36.66 ± 0.23
SES (Ours)	$\mathbf{49.00 \pm 0.08}$	$\mathbf{48.22 \pm 0.54}$	$\mathbf{45.94 \pm 0.27}$	$\mathbf{43.63 \pm 1.00}$	$\mathbf{41.82 \pm 0.43}$	$\mathbf{39.88 \pm 0.7}$	$\mathbf{38.16 \pm 0.38}$

Table 14: Results on text classification (IMDB). The best one is **bold**, and the runner-up is underlined.

Dataset	IMDB Review(100%:95.90)						
Sampling rate	70%	50%	20%	10%	5%	2%	1%
Random	95.25 ± 0.21	95.04 ± 0.31	93.53 ± 0.68	91.89 ± 0.17	89.60 ± 1.89	83.25 ± 4.96	73.31 ± 1.94
Moderate	95.39 ± 0.19	95.31 ± 0.07	94.03 ± 0.73	92.55 ± 0.47	90.34 ± 0.43	58.34 ± 4.29	50.81 ± 0.55
CCS	95.22 ± 0.18	95.35 ± 0.19	93.44 ± 0.61	91.87 ± 0.23	89.89 ± 1.47	85.73 ± 4.76	82.05 ± 4.21
$\mathbb{D}^2$ Pruning	95.43 ± 0.16	95.40 ± 0.20	93.75 ± 0.46	92.44 ± 0.60	90.77 ± 0.33	87.40 ± 0.78	80.06 ± 0.85
GraphCut	95.39 ± 0.15	95.21 ± 0.29	93.37 ± 0.57	91.69 ± 0.66	90.93 ± 0.31	86.85 ± 1.81	82.26 ± 0.90
Entropy	95.39 ± 0.31	95.17 ± 0.22	93.92 ± 0.50	92.57 ± 0.97	90.30 ± 0.63	77.16 ± 4.52	59.41 ± 4.70
Forgetting	95.41 ± 0.11	95.31 ± 0.17	93.66 ± 0.30	89.41 ± 0.58	58.78 ± 2.28	55.81 ± 4.65	52.38 ± 1.03
EL2N	95.29 ± 0.19	95.34 ± 0.21	91.31 ± 0.19	60.29 ± 0.09	49.88 ± 1.35	47.18 ± 3.30	43.74 ± 0.81
AUM	95.27 ± 0.66	95.23 ± 0.16	90.60 ± 0.13	55.68 ± 0.21	49.81 ± 1.50	43.13 ± 4.53	36.29 ± 1.45
Variance	95.44 ± 0.16	95.40 ± 0.20	93.75 ± 0.46	92.44 ± 0.60	90.77 ± 0.33	87.40 ± 0.78	80.06 ± 0.85
***k*-means**	95.34 ± 0.17	95.22 ± 0.23	93.98 ± 0.54	92.49 ± 0.74	90.21 ± 0.88	86.96 ± 1.84	81.51 ± 6.72
***k*-DPP**	95.29 ± 0.37	95.13 ± 0.21	93.76 ± 0.59	92.50 ± 0.58	89.97 ± 1.42	86.14 ± 2.53	77.07 ± 3.31
SES (Ours)	$\mathbf{95.60 \pm 0.16}$	$\mathbf{95.40 \pm 0.12}$	$\mathbf{94.57 \pm 0.09}$	$\mathbf{92.96 \pm 0.56}$	$\mathbf{91.42 \pm 0.24}$	$\mathbf{88.58 \pm 0.47}$	$\mathbf{83.14 \pm 2.05}$

Table 15: Results on object detection. The best one is **bold**, and the runner-up is underlined.

Dataset	PASCAL VOC (100%:76.29)						
Sampling rate	70%	50%	20%	10%	5%	2%	1%
Random	74.02 ± 0.26	72.10 ± 0.32	65.45 ± 0.45	57.56 ± 0.45	43.47 ± 0.67	18.78 ± 0.21	9.24 ± 0.96
Moderate	73.42 ± 0.46	72.03 ± 0.52	65.12 ± 0.57	54.71 ± 0.10	40.20 ± 0.54	15.97 ± 0.36	5.13 ± 0.49
CCS	74.64 ± 0.15	72.27 ± 0.23	65.72 ± 0.59	57.35 ± 0.63	39.01 ± 0.81	17.26 ± 0.62	8.49 ± 0.57
$\mathbb{D}^2$ Pruning	74.46 ± 0.52	72.55 ± 0.23	65.59 ± 0.84	55.73 ± 0.34	44.04 ± 0.41	19.16 ± 0.14	10.75 ± 0.75
GraphCut	67.45 ± 0.35	64.15 ± 0.54	53.12 ± 0.30	38.29 ± 0.12	26.81 ± 0.32	8.56 ± 0.64	8.16 ± 0.54
AL-MDN	74.51 ± 0.35	70.36 ± 0.17	65.26 ± 0.82	54.51 ± 0.94	30.85 ± 1.71	12.33 ± 1.44	8.97 ± 1.33
***k*-means**	74.22 ± 0.31	72.35 ± 0.19	65.52 ± 0.98	57.01 ± 0.49	43.35 ± 0.60	16.96 ± 0.78	5.16 ± 0.69
***k*-DPP**	74.19 ± 0.38	71.99 ± 0.27	65.39 ± 0.53	56.80 ± 0.17	43.92 ± 0.53	18.20 ± 0.44	10.50 ± 0.62
SES (Ours)	$\mathbf{75.20 \pm 0.29}$	$\mathbf{73.33 \pm 0.33}$	$\mathbf{66.52 \pm 0.41}$	$\mathbf{59.52 \pm 0.14}$	$\mathbf{45.92 \pm 0.46}$	$\mathbf{23.39 \pm 0.22}$	$\mathbf{16.15 \pm 0.62}$

Table 16: Results on visual question answering. The best one is **bold**, and the runner-up is underlined.

Dataset	CC SBU Align (100%:30.40)						
Sampling rate	70%	50%	20%	10%	5%	2%	1%
Random	29.66 ± 0.15	29.62 ± 0.05	29.21 ± 0.26	29.01 ± 0.14	28.20 ± 0.12	25.51 ± 0.46	25.11 ± 0.42
Moderate	29.96 ± 0.14	29.67 ± 0.13	29.53 ± 0.27	29.11 ± 0.23	27.30 ± 0.25	24.85 ± 0.36	26.54 ± 0.41
CCS	29.93 ± 0.06	29.90 ± 0.05	29.94 ± 0.16	29.91 ± 0.25	27.71 ± 0.37	25.31 ± 0.37	25.59 ± 0.41
$\mathbb{D}^2$ Pruning	30.09 ± 0.13	29.97 ± 0.19	29.44 ± 0.22	29.30 ± 0.27	26.44 ± 0.23	25.03 ± 0.30	26.29 ± 0.37
GraphCut	29.86 ± 0.08	29.73 ± 0.06	29.53 ± 0.23	29.11 ± 0.25	27.30 ± 0.36	24.85 ± 0.41	26.54 ± 0.29
Instruction	30.12 ± 0.15	29.93 ± 0.25	29.82 ± 0.27	29.01 ± 0.28	26.76 ± 0.42	23.72 ± 0.49	24.60 ± 0.46
***k*-means**	29.78 ± 0.14	29.61 ± 0.14	29.54 ± 0.11	29.20 ± 0.20	27.72 ± 0.35	25.47 ± 0.39	25.60 ± 0.41
***k*-DPP**	29.33 ± 0.15	29.55 ± 0.12	29.48 ± 0.08	29.27 ± 0.12	28.16 ± 0.34	25.93 ± 0.46	26.13 ± 0.34
SES (Ours)	$\mathbf{30.25 \pm 0.10}$	$\mathbf{30.20 \pm 0.13}$	$\mathbf{30.21 \pm 0.18}$	$\mathbf{30.10 \pm 0.11}$	$\mathbf{28.23 \pm 0.40}$	$\mathbf{27.19 \pm 0.46}$	$\mathbf{27.61 \pm 0.39}$

F.2 Active Learning

We present detailed experimental results for active learning in Table 17. Our method consistently performs better than baselines across all sampling rates.

Table 17: Results for active learning. The best one is **bold**, and the runner-up is underlined.

Dataset	ImageNet-1K (100%:73.63)						
Sampling rate	70%	50%	20%	10%	5%	2%	1%
Random	71.12 ± 0.25	69.43 ± 0.04	58.77 ± 0.35	47.36 ± 0.20	33.41 ± 0.15	16.41 ± 0.40	5.41 ± 0.23
Moderate	71.48 ± 0.05	68.68 ± 0.06	56.35 ± 0.01	42.29 ± 0.17	26.77 ± 0.01	11.37 ± 0.22	4.22 ± 0.17
CCS	71.46 ± 0.11	69.50 ± 0.07	58.85 ± 0.16	45.06 ± 0.22	28.02 ± 0.17	9.03 ± 0.40	2.33 ± 0.18
GraphCut	71.50 ± 0.21	69.16 ± 0.09	56.08 ± 0.24	40.99 ± 0.21	24.30 ± 0.17	7.90 ± 0.13	2.46 ± 0.08
$\mathbb{D}^2$ Pruning	71.62 ± 0.11	69.02 ± 0.21	59.65 ± 0.11	45.97 ± 0.32	28.08 ± 0.37	14.24 ± 0.11	4.79 ± 0.31
Prototypicality	70.12 ± 0.04	66.00 ± 0.06	49.20 ± 0.09	35.27 ± 0.04	24.14 ± 0.15	13.88 ± 0.08	4.95 ± 0.05
SES (Ours)	$\mathbf{72.11 \pm 0.07}$	$\mathbf{70.15 \pm 0.17}$	$\mathbf{60.22 \pm 0.34}$	$\mathbf{48.10 \pm 0.21}$	$\mathbf{34.82 \pm 0.22}$	$\mathbf{17.97 \pm 0.35}$	$\mathbf{6.69 \pm 0.62}$

F.3 Continual Learning

In addition to baselines from Sec. 5.1, we include six widely used baseline selection methods for continual learning: 1) ***k*-center** (Sener & Savarese, 2018), which iteratively selects samples

that are least similar to those already selected, 2) **Gradient matching** (Campbell & Broderick, 2019), which selects samples whose average gradient closely approximates the average gradient of all samples, 3) **FRCL** (Titsias et al., 2020), which optimizes a subset of samples to minimize the posterior uncertainty of the Gaussian process induced from the embedding representations, 4) **iCaRL** (Rebuffi et al., 2017) that selects samples whose average embedding closely approximates the average embedding of all samples, 5) **Greedy Coreset** (Borsos et al., 2020) that formulates the selection as a bilevel optimization problem and greedily selects samples such that the model trained on them minimizes the loss across the entire dataset, and 6) **BCSR** (Hao et al., 2024) that formulates the selection as a bilevel optimization problem on the probability simplex over samples and introduces a regularizer to control the number of selected samples.

We present detailed experimental results for continual learning in Table 18 and 19. Our method consistently performs better than baselines across all datasets and memory sizes.

Table 18: Results for continual learning on Permuted MNIST, Split MNIST, and Split CIFAR10. The best one is **bold**, and the runner-up is underlined.

Dataset	Permuted MNIST				Split MNIST				Split CIFAR10			
Memory size	50	100	200	400	50	100	200	400	50	100	200	400
Random	75.99 ± 0.70	77.43 ± 0.41	79.69 ± 0.44	81.32 ± 0.33	92.66 ± 1.46	95.79 ± 0.30	97.16 ± 0.13	98.18 ± 0.50	62.49 ± 0.73	62.34 ± 0.89	63.69 ± 1.58	63.63 ± 0.86
Moderate	76.34 ± 0.59	78.29 ± 0.52	79.44 ± 0.31	78.88 ± 0.62	92.74 ± 0.59	95.34 ± 0.18	97.05 ± 0.07	97.61 ± 0.44	61.55 ± 0.61	61.51 ± 0.46	63.01 ± 0.58	65.42 ± 3.68
CCS	74.28 ± 0.75	75.48 ± 0.46	76.53 ± 0.53	81.64 ± 0.16	80.62 ± 1.01	89.50 ± 0.92	94.92 ± 0.76	98.34 ± 0.17	61.14 ± 0.92	60.56 ± 1.27	61.04 ± 1.73	59.33 ± 1.21
$\mathbb{D}^2$ Pruning	77.19 ± 0.46	78.25 ± 0.30	79.94 ± 0.36	80.93 ± 0.12	93.92 ± 0.22	96.79 ± 0.12	97.69 ± 6.88	98.07 ± 0.08	61.90 ± 1.41	64.54 ± 0.63	66.08 ± 1.45	65.23 ± 1.18
GraphCut	75.31 ± 0.42	76.98 ± 6.74	78.61 ± 0.36	80.39 ± 0.29	88.37 ± 0.37	91.34 ± 1.09	94.25 ± 0.71	98.44 ± 0.20	60.46 ± 1.29	61.02 ± 1.17	61.66 ± 1.67	63.51 ± 0.77
Entropy	76.74 ± 0.35	75.54 ± 0.35	78.18 ± 0.44	82.08 ± 0.19	94.33 ± 0.34	91.54 ± 0.73	96.16 ± 0.26	98.27 ± 0.11	61.78 ± 0.44	61.53 ± 0.72	62.72 ± 0.73	63.99 ± 1.01
Forgetting	74.38 ± 0.54	75.30 ± 0.25	77.47 ± 0.40	79.13 ± 0.70	89.00 ± 2.43	92.13 ± 0.43	96.37 ± 0.20	98.25 ± 0.18	60.81 ± 0.78	59.56 ± 0.24	61.38 ± 1.22	61.59 ± 1.07
EL2N	73.32 ± 0.80	75.57 ± 0.24	77.48 ± 0.20	80.34 ± 0.47	83.56 ± 1.05	88.54 ± 1.01	94.87 ± 0.48	97.45 ± 0.13	59.00 ± 0.54	57.79 ± 0.75	58.34 ± 0.68	58.58 ± 1.34
AUM	73.98 ± 0.79	75.54 ± 0.35	77.47 ± 0.33	79.90 ± 0.61	82.31 ± 2.15	90.38 ± 1.99	95.79 ± 0.34	98.07 ± 0.24	58.95 ± 0.77	58.32 ± 0.46	58.06 ± 0.86	59.01 ± 0.67
Variance	74.53 ± 0.47	75.67 ± 0.38	77.42 ± 0.32	78.70 ± 0.34	84.08 ± 3.14	91.90 ± 0.72	94.96 ± 0.88	97.49 ± 0.38	58.57 ± 0.57	58.69 ± 0.24	57.77 ± 0.34	58.50 ± 0.74
***k*-center**	75.64 ± 0.40	78.17 ± 0.23	79.75 ± 0.17	80.94 ± 0.38	90.41 ± 1.23	94.39 ± 0.41	96.61 ± 0.64	97.80 ± 0.13	61.99 ± 1.36	61.47 ± 1.71	62.74 ± 1.31	64.45 ± 2.24
Gradient Matching	75.73 ± 0.57	77.30 ± 0.08	79.27 ± 0.38	80.71 ± 0.50	91.58 ± 1.06	95.39 ± 0.93	97.54 ± 0.23	98.39 ± 0.26	60.54 ± 0.92	61.65 ± 6.98	62.65 ± 1.11	63.26 ± 0.96
FRCL	75.78 ± 0.46	77.33 ± 0.26	79.21 ± 0.53	80.88 ± 0.30	88.46 ± 0.61	94.48 ± 0.93	97.10 ± 0.31	98.33 ± 0.20	61.22 ± 1.61	61.67 ± 1.02	62.93 ± 0.86	65.51 ± 1.57
iCaRL	77.01 ± 0.19	78.94 ± 0.46	80.65 ± 0.36	81.94 ± 0.14	92.92 ± 1.23	89.50 ± 0.92	97.59 ± 8.14	98.39 ± 0.05	61.95 ± 1.09	62.33 ± 0.89	64.08 ± 1.58	64.09 ± 1.15
Greedy Coreset	77.19 ± 0.56	78.71 ± 0.67	80.13 ± 0.11	82.17 ± 0.33	94.35 ± 0.35	96.07 ± 0.42	97.76 ± 0.85	98.18 ± 0.16	61.28 ± 1.74	63.18 ± 0.84	62.98 ± 0.91	65.02 ± 1.50
BCSR	75.92 ± 0.35	77.74 ± 0.39	79.51 ± 0.28	81.65 ± 0.09	93.83 ± 1.18	94.77 ± 0.56	96.98 ± 0.29	98.26 ± 0.11	61.88 ± 0.59	63.23 ± 2.60	64.59 ± 2.86	65.45 ± 0.70
SES (Ours)	$\mathbf{78.52 \pm 0.25}$	$\mathbf{79.92 \pm 0.36}$	$\mathbf{81.18 \pm 0.26}$	$\mathbf{82.69 \pm 0.10}$	$\mathbf{94.73 \pm 0.33}$	$\mathbf{96.94 \pm 0.34}$	$\mathbf{98.28 \pm 0.10}$	$\mathbf{98.54 \pm 0.07}$	$\mathbf{67.52 \pm 0.56}$	$\mathbf{68.26 \pm 1.24}$	$\mathbf{69.32 \pm 0.99}$	$\mathbf{70.76 \pm 1.22}$

Table 19: Results for continual learning on Split CIFAR100 and Split Tiny-ImageNet. The best one is **bold**, and the runner-up is underlined.

Dataset	Split CIFAR100				Split Tiny-ImageNet			
Memory size	50	100	200	400	50	100	200	400
Random	46.59 ± 1.28	51.29 ± 0.77	54.22 ± 0.58	56.21 ± 0.46	18.38 ± 0.26	18.52 ± 0.23	19.22 ± 0.29	19.22 ± 0.26
Moderate	47.38 ± 0.39	51.91 ± 0.63	53.45 ± 8.69	55.06 ± 0.86	18.08 ± 0.30	18.63 ± 0.36	19.47 ± 6.18	19.75 ± 0.24
CCS	44.91 ± 0.35	48.70 ± 6.90	51.26 ± 0.39	52.69 ± 0.29	18.47 ± 0.41	18.30 ± 0.17	18.90 ± 0.13	18.50 ± 0.22
$\mathbb{D}^2$ Pruning	47.72 ± 0.61	51.86 ± 0.62	54.50 ± 0.46	57.14 ± 0.42	18.98 ± 0.10	19.08 ± 0.39	19.50 ± 0.28	19.76 ± 0.14
GraphCut	48.72 ± 0.56	53.35 ± 0.38	54.66 ± 0.28	56.74 ± 0.36	19.50 ± 0.19	19.76 ± 6.15	20.53 ± 0.12	21.57 ± 0.36
Entropy	45.08 ± 1.86	47.97 ± 1.34	51.51 ± 0.34	54.42 ± 0.69	18.38 ± 0.42	17.99 ± 0.28	18.62 ± 0.22	19.20 ± 0.25
Forgetting	50.60 ± 1.08	53.06 ± 0.57	54.68 ± 0.31	57.30 ± 0.30	18.92 ± 0.19	19.55 ± 0.13	19.56 ± 0.33	19.85 ± 0.30
EL2N	44.76 ± 1.10	46.47 ± 0.62	48.11 ± 1.01	50.59 ± 0.64	18.04 ± 0.35	17.95 ± 0.31	17.98 ± 0.32	18.37 ± 0.24
AUM	44.70 ± 0.73	46.14 ± 0.58	47.20 ± 0.40	49.24 ± 0.88	18.36 ± 0.41	18.24 ± 0.10	17.89 ± 0.17	18.16 ± 0.21
Variance	50.30 ± 0.84	52.83 ± 0.76	54.00 ± 0.85	56.91 ± 0.28	19.66 ± 0.42	19.32 ± 0.07	19.50 ± 0.33	20.19 ± 0.13
***k*-center**	46.90 ± 1.86	51.16 ± 0.57	53.10 ± 0.17	55.77 ± 0.34	18.81 ± 0.21	18.87 ± 0.18	18.90 ± 0.30	19.13 ± 0.14
Gradient Matching	51.15 ± 0.66	54.13 ± 0.53	56.29 ± 0.26	57.24 ± 0.37	19.20 ± 0.32	19.19 ± 8.72	19.00 ± 0.16	19.46 ± 0.18
FRCL	46.81 ± 0.71	51.40 ± 0.44	54.28 ± 0.55	56.01 ± 0.62	18.59 ± 0.21	18.86 ± 0.15	19.01 ± 0.27	19.55 ± 0.20
iCaRL	51.67 ± 0.71	54.62 ± 0.51	56.11 ± 0.32	56.95 ± 0.26	19.05 ± 0.45	19.58 ± 0.18	19.85 ± 0.16	19.86 ± 0.58
Greedy coreset	52.58 ± 0.39	56.17 ± 0.42	57.72 ± 0.23	55.27 ± 0.66	19.61 ± 0.28	19.24 ± 0.34	19.98 ± 0.17	20.62 ± 0.36
BCSR	47.37 ± 1.25	50.21 ± 1.14	51.49 ± 0.62	59.45 ± 0.42	19.04 ± 0.36	18.75 ± 0.17	18.74 ± 0.26	19.42 ± 0.17
SES (Ours)	$\mathbf{54.71 \pm 0.53}$	$\mathbf{57.60 \pm 0.39}$	$\mathbf{59.69 \pm 0.31}$	$\mathbf{61.06 \pm 0.17}$	$\mathbf{20.40 \pm 0.34}$	$\mathbf{20.80 \pm 0.18}$	$\mathbf{21.20 \pm 0.12}$	$\mathbf{21.82 \pm 0.20}$

G Additional Ablation Study

Robustness to different training difficulty metrics. We test the effect of using different training difficulty metrics, including Forgetting, EL2N, and AUM. We also include the identity baseline, which assigns identical scores to all samples. Table 20 shows the results. Using identical scores leads to inferior performance, indicating the importance of incorporating training difficulty. Meanwhile, using AUM, Forgetting, and EL2N yields comparable performance, with average accuracies across rates differing by no more than 0.5%. This demonstrates the robustness of our method to the choice of the training difficulty metric.

Table 20: Ablation of training difficulty metrics. The best one is **bold**, and the runner-up is underlined.

Difficulty metric	Sampling rate							Avg.
	70%	50%	20%	10%	5%	2%	1%	
Identity	94.58	92.66	86.67	78.50	67.68	53.21	44.43	73.96
Forgetting	94.86	93.99	88.11	79.06	**70.45**	53.99	**46.43**	75.27
EL2N	94.61	93.74	**88.45**	79.93	69.52	54.01	45.15	75.06
AUM	**95.01**	**94.50**	88.31	**80.24**	69.82	**54.78**	45.25	**75.42**

Quantification of node-level structural entropy. In Eq. (4), we quantify the node-level structural entropy as $S_e(u) = \frac{1}{vol(V)} \sum_{\langle u,v \rangle \in E} w_{u,v} \log vol(\alpha_{u \vee v})$ by removing the second term from Eq. (3). Alternatively, the node-level structural entropy can retain the second term and be quantified as $S_e(u) = \frac{1}{vol(V)} (\sum_{\langle u,v \rangle \in E} w_{u,v} \log vol(\alpha_{u \vee v}) - d(u) \log d(u))$. As shown in Table 21, removing the second term slightly increases performance across all sampling rates. This finding supports our decision to remove the second term in the definition of node-level structural entropy.

Table 21: Ablation on the quantification of node-level structural entropy. The best one is **bold**, and the runner-up is underlined.

Quantification method	Sampling rate						
	70%	50%	20%	10%	5%	2%	1%
With the second term	94.51	93.39	88.01	79.73	67.75	53.88	43.02
Without the second term	**95.01**	**94.50**	**88.31**	**80.24**	**69.82**	**54.78**	**45.25**

Methods for combining global and local metrics. We explore possible alternative methods to combine the global metric $S_e(u)$ and the local metric $S_t(u)$ other than the proposed multiplication. Specifically, we experimented with the sum $(S_e(u) + S_t(u))$, the harmonic mean $(\frac{S_e(u)S_t(u)}{S_e(u)+S_t(u)})$, and the maximum $(\max(S_e(u), S_t(u)))$. As shown in Table 22, multiplication achieves the best average performance, validating our choice for combining the two metrics.

Table 22: Ablation on different combination of S_e and S_t. The best one is **bold**, and the runner-up is underlined.

Combination method	Sampling rate							Avg.
	70%	50%	20%	10%	5%	2%	1%	
$S_e(u) + S_t(u)$	94.77	94.43	87.17	79.64	69.08	53.24	44.53	71.35
$\frac{S_e(u)S_t(u)}{S_e(u)+S_t(u)}$	94.84	**94.64**	88.11	79.97	69.75	53.95	44.88	71.88
$\max(S_e(u), S_t(u))$	94.22	93.22	87.24	78.33	68.49	53.04	43.30	70.60
$S_e(u) \cdot S_t(u)$	**95.01**	94.50	**88.31**	**80.24**	**69.82**	**54.78**	**45.25**	**72.15**

Replacing graphs with hypergraphs. We have conducted an experiment using hypergraphs (Zhou et al., 2006) to capture the relationships between samples. Following Feng et al. (2019), we construct a hypergraph by adding a hyperedge for each node that contains the node itself and its k-nearest neighbors. Due to the lack of the structural entropy theory for hypergraphs, we apply clique expansion (Agarwal et al., 2006), creates an edge between every pair of nodes in a hyperedge, to convert the hypergraph into a graph. We then apply our selection method to the resulting graph. Table 23 shows the results. This hypergraph-based method slightly degrades performance compared to the graph-based method, but still performs better than the baseline methods in low-sampling-rate settings. We attribute this slight decline in performance to the information loss during clique expansion, for which a straightforward alternative is not currently available. We see significant potential for future work in developing structural entropy theories for hypergraphs and then applying our method to sample selection.

Table 23: Ablation study on replacing graphs with hypergraphs. The best one is **bold**, and the runner-up is underlined.

Graph Type	Sampling rate						
	70%	50%	20%	10%	5%	2%	1%
Hypergraph	94.81	94.37	88.12	80.05	69.30	54.50	44.72
Graph	**95.01**	**94.50**	**88.31**	**80.24**	**69.82**	**54.78**	**45.25**

H Full Qualitative results

Fig. 6 visualizes the results of different methods when selecting 2% of the samples from CIFAR10. Methods that select the most difficult samples, such as AUM, oversample near several class boundaries and undersample in several classes that are easier to classify. Methods that prioritize sample coverage, such as $\mathbb{D}^2$ Pruning and CCS, achieve a better sample coverage but may undersample near several class boundaries and fail to preserve the global structure. Our method well covers the data distribution, providing a set of informative and representative samples for model training.

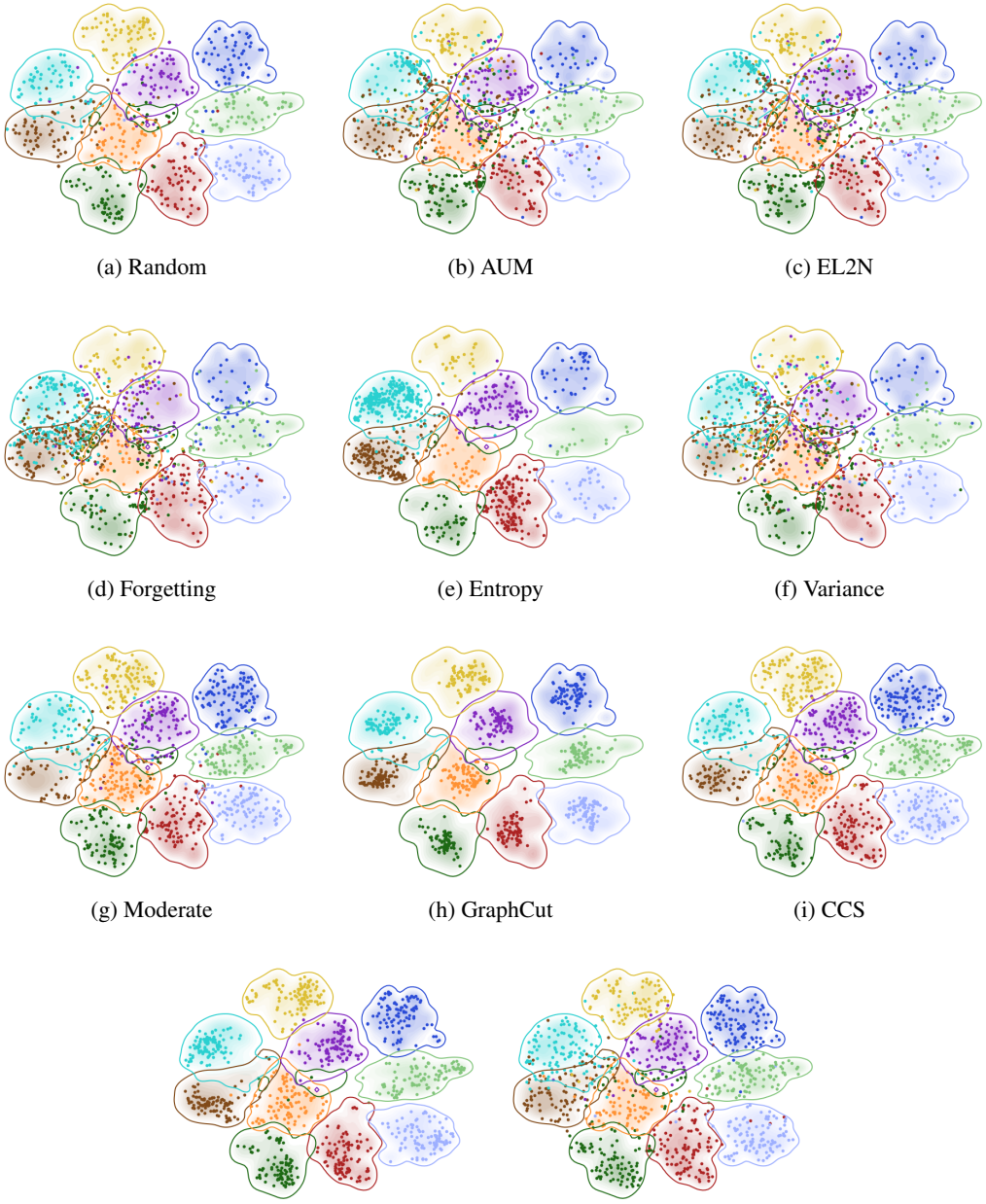

(a) Random (b) AUM (c) EL2N

(d) Forgetting (e) Entropy (f) Variance

(g) Moderate (h) GraphCut (i) CCS

(j) $\mathbb{D}^2$ Pruning (k) SES (Ours)

Figure 6: Visualizations of selection results of different methods when selecting 2% of the samples from CIFAR10.